eLife

Reviewed Preprint
v1 • January 28, 2026
Not revised

Reviewed Preprint
v2 • July 23, 2026
Revised by authors

RiboTRAP-seq identifies spatially distinct functions for the anterior and posterior intestine in immune and metabolic regulation in *C. elegans*

Chung-Chih Liu[*,†], **Nicolas Seban**[*,‡], **Supriya Srinivasan**

Department of Neuroscience and Dorris Neuroscience Center, The Scripps Research Institute, La Jolla, United States

For correspondence: supriya@scripps.edu

[*] These authors contributed equally

[†] Current affiliation: Department of Molecular Biology, University of Texas Southwestern Medical Center, Dallas, United States

[‡] Current affiliation: UC Davis Center for Neuroscience, Davis, United States

Competing interests: No competing interests declared

Funding: See page 35

Reviewing editor: Sylvia Lee, Cornell University, United States

eLife Assessment

In this **valuable** study, the authors performed cell-specific ribosome pulldown to identify gene expression (translatome) differences in the anterior (NT1) vs middle & posterior (NT2-9) cells of the C. elegans intestine, under fed, starved, or refeeding conditions. The data generated will be very helpful to the C. elegans community, and the evidence supporting the conclusions of the study is assessed to be **solid**. Some methodological caveats remain and are discussed.

https://doi.org/10.7554/eLife.109237.2.sa3

Abstract

The intestine integrates food-derived cues to coordinate organismal physiology, yet the molecular specialization of discrete regions along the intestinal epithelium remains unclear. Here, we generate cell type-specific translatomes of the *Caenorhabditis elegans* intestine during fasting and refeeding using discrete promoters for the anterior quartet of intestinal cells (INT1) and the remaining 8 pairs of intestinal cells (INT2-9). We found that the anterior-most INT1 cells are a translationally distinct intestinal sub-compartment that is particularly enriched for immune-and stress-response genes. Functional assays using novel INT1-specific genes emerging from this study reveal that these specialized cells play a previously unappreciated role in pathogen avoidance and organismal survival. A second critical function of INT1 cells is their role in sensing and responding to the contents of the gut lumen. We show that luminal pyruvate is the key signal linking bacterial nutrients in the gut, to secretion of the gut insulin antagonist INS-7. These findings establish INT1 as sentinel enteroendocrine cells that integrate metabolic and immune cues to couple food status with immune and endocrine responses. Our studies also provide a rich resource for dissecting segment-specific intestinal biology, an overlooked and fertile area for future research.

Introduction

The intestine is a critical organ for food digestion and nutrient absorption in animals. *Caenorhabditis elegans*, as a bacterivore, constantly ingests a variety of bacteria with an intestinal transit time as short as two minutes in adults [1]. This rapid process implies the existence of food-sensing mechanisms within the intestine that can continuously monitor and respond to the acute fluctuation in food availability. When food is absent, a transcriptional metabolic response is evoked via the induction of the fasting response genes including lipases, peroxisomal and mitochondrial β-oxidation genes and some fatty acid desaturases in the intestine to maintain energy homeostasis [2–4]. However, it has been unclear whether discrete segments within the intestine have specific food-sensing capabilities or exhibit different responses to fasting in comparison to the organ as a whole. To our knowledge, no studies to date have addressed this question with high spatial and temporal resolution. The *C. elegans* intestine is comprised of 20 cells

designated INT1-INT9 [5]. The anterior ring comprises 4 cells called INT1, which are the most proximal intestinal cells adjacent to the pharynx and represent the initial location of contact with ingested food, which for *C. elegans* is digested bacterial components. The remaining 16 cells are arranged in pairs to form the latter 8 posterior rings (INT2-9) arranged in a stereotypical structure. A number of years ago *Sulston et al.* had observed that the microvilli of INT1 cells are shorter than those in the rest of the intestine [5], which implies that INT1 cells may not have the same food absorption capacity that INT2-9 cells have.

In addition to the morphological differences, we recently reported that INT1 functions as an enteroendocrine cell, and secretes the gut peptide INS-7 shortly after food withdrawal. INS-7 secretion levels increase over the duration of fasting, which are reset by the re-introduction of food. Gut INS-7 acts in the nervous system to suppress the fat loss-stimulating peptide FLP-7, functional ortholog of the *C. elegans* tachykinin peptide [6]. This mechanism allows the stimulation of fat loss to be regulated, in part, by incoming food signals from the gut. Furthermore, *Quintin et al.* showed that worms treated with H_2O_2 have an induction of the antioxidant enzyme PRDX-2 specifically in INT1 cells, suggesting that INT1 cells may have additional oxidative stress-sensing functions [7]. Although these lines of evidence have suggested that INT1 cells may be a group of specialized intestinal cells that sense the quality of the ingested food and have distinct fasting responses, many questions remain. First, the molecular features of INT1 cells and the molecular distinctions between INT1 and the rest of the intestine (INT2-9) have not been defined. Second, the role of INT1 cells in modulating physiological responses to changes in food availability remains undetermined. Finally, the differential effects of metabolic challenge via fasting and re-feeding in the subsets of intestinal cells are unclear.

In this study, we aim to address these questions using spatial translatomics. In short, the approach is as follows: actively translating mRNAs are bound to clusters of ribosomes, referred to as polysomes [8, 9]. Translating ribosome affinity purification (TRAP) was developed to isolate cell type-specific polysome-mRNA complexes [10, 11], allowing quantitative analysis of translational regulation [12]. Here, we performed TRAP-Seq using a modified protocol based on *McLachlan et al.* [13], in which RPL-22 was tagged with HA to enable affinity purification of polysome-mRNA complexes, which is followed by RNA sequencing. This approach provided a comprehensive spatially distinct translatomic profile of actively translating mRNAs in INT1 and INT2-9 cells. To discern novel temporal features in response to metabolic challenge, we examined the translational responses of these intestinal subsets to acute and chronic fasting and refeeding paradigms. Our datasets reveal that INT1 cells exhibit a distinct molecular identity, characterized by the enrichment of immune- and stress-responsive genes. Furthermore, fasting and refeeding elicit divergent regulatory programs in INT1 and INT2-9 cells. To our knowledge, this represents the first study to determine the molecular identities of discrete intestinal cell subsets in response to fasting and refeeding in *C. elegans*.

Results

Isolation and sequencing of translating RNA from INT1 and INT2-9 cells

To identify the molecular differences between INT1 and INT2-9 cells in fed, fasted and refed states, we employed translating ribosome affinity purification (TRAP) [10, 11] to isolate polysomal RNA from INT1 and INT2-9 cells followed by RNA sequencing. This approach captures actively translating mRNAs, thereby providing a cell type-specific snapshot of the translational landscape under fasting and refeeding conditions. To selectively target INT1 and INT2-9 cells, we expressed the HA-tagged ribosomal protein (RPL-22-3xHA) under the control of the *Pges-111B* [6, 14] and *Ppho-1* [15] promoters, respectively. As published [6], we noted that *Pges-111B* is strictly expressed in INT1 cells, whereas *Ppho-1* is expressed in INT2-9 cells with detectable, albeit lower expression in INT2 cells (Fig 1A).

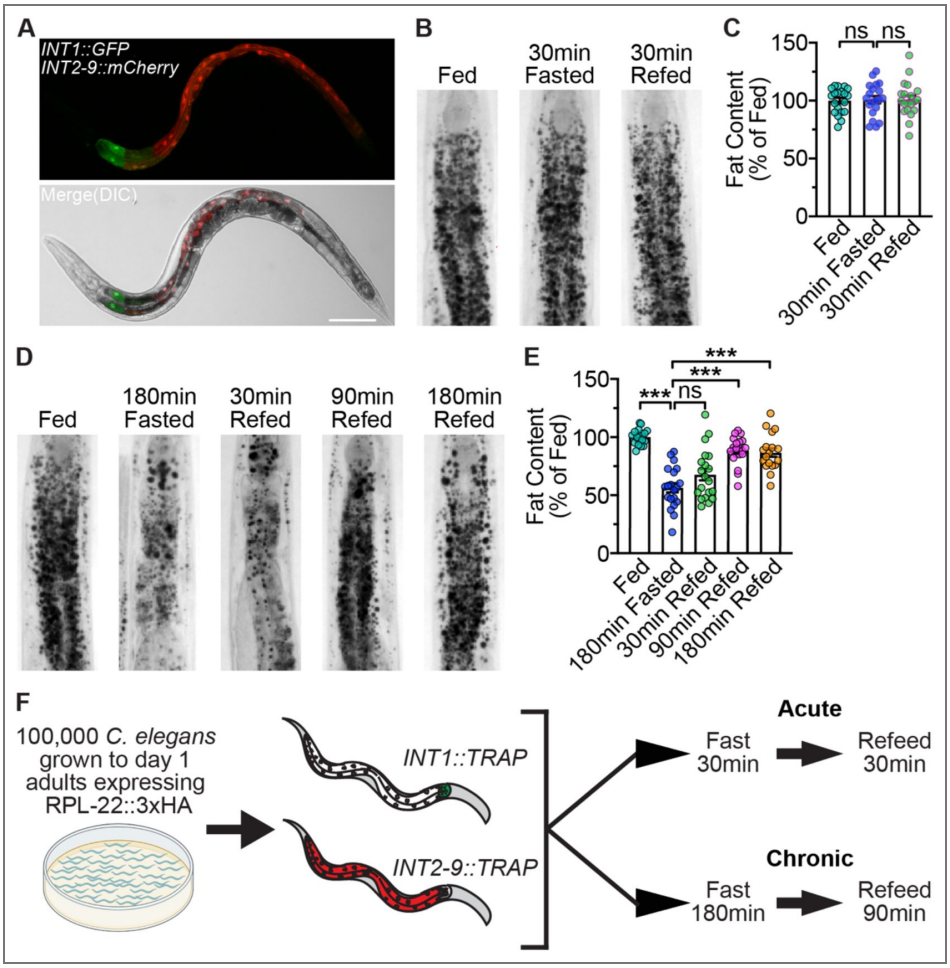

Fig 1. Conditions and workflow for INT1- and INT2-9-specific translatomics.

(A) Representative images of wild-type animals bearing integrated *INT1::GFP* and *INT2-9::mCherry* transgenes. Upper panel, GFP expression in INT1 cells and mCherry expression in INT2-9 cells; lower panel, merge with DIC. Scale bar, 100 μm. (B) Representative images of wild-type animals in fed, 30 min fasted, and 30 min refed states fixed and stained with Oil Red O. (C) Fat content was quantified for each condition and expressed as a percentage of wild-type animals in fed state ± SEM (n=20). $^{ns}p>0.05$ by one-way ANOVA (Tukey). (D) Representative images of wild-type animals in fed, 180 min fasted, 30 min refed, 90 min refed, and 180 min refed states fixed and stained with Oil Red O. (E) Fat content was quantified for each condition and expressed as a percentage of wild-type animals in fed state ± SEM (n=18-20). ***p<0.001, $^{ns}p>0.05$ by one-way ANOVA (Sidak). (F) 100000 *C. elegans* expressing *INT1::RPL-22::3xHA* or *INT2-9::RPL-22::3xHA* were grown to day 1 adults. Worms were fasted and refed for the time indicated and harvested for TRAP-Seq. Created with *BioRender.com*.

We operationally defined the 'acute' conditions at 30 min fasting followed by 30 min refeeding, because under these conditions, intestinal fat content remains unchanged (Fig 1B and 1C). However, INS-7 secretion was induced within the 30 min acute fasting period and restored to baseline levels within 30 min upon refeeding [6], indicating that intestinal responses to food withdrawal can occur before detectable changes in lipid stores. Chronic conditions were established as 3 hr fasting followed by 90 min refeeding. In this paradigm, animals lost approximately half of intestinal lipid stores after chronic fasting, which were subsequently replenished upon refeeding for 90 min (Fig 1D and 1E). Thus, chronic conditions represent a more pronounced metabolic challenge. For TRAP-Seq sample preparation, we cultured 100,000 *INT1::TRAP* or *INT2-9::TRAP* animals to the Day 1 adult stage, subjected them to acute or chronic conditions (Fig 1F), and performed RNA isolation following a modified TRAP protocol [13]. These experiments were conducted 3 times.

Stress response genes distinguish INT1 from INT2-9 translatomes across acute and chronic conditions

Principal component analysis (PCA) of all TRAP-Seq datasets revealed clearly distinct clustering by promoter identity, indicating that INT1 and INT2-9 cells maintain fundamentally different molecular identities independent of any and all acute or chronic conditions (Fig 2A). We found PC2 to be significantly associated with promoter identity (FDR = 1.2e-10, Pearson's correlation) and PC1 with metabolic stress (FDR = 1.4e-6, ANOVA). To systematically define these differences, we performed weighted correlation network analysis (WGCNA) [16], which unbiasedly identified 12 gene modules associated with condition-specific responses across the INT1 and INT2-9 datasets (Fig 2B and 2C, S1A Fig). Notably, the expression of genes in module red was positively correlated to all INT1 conditions but negatively correlated to all INT2-9 conditions, suggesting a transcriptional program preferentially translated in INT1 cells (Fig 2C and S1A Fig). Examination of normalized counts confirmed uniformly higher expression of module red genes across all INT1 conditions compared with INT2-9 (Fig 2D). To identify the categories and functions of module red genes, we used WormCat [17, 18], an annotation and category enrichment tool with near-complete annotation of the *C. elegans* genome. Among the 100 genes from module red, we found genes involved in "Stress Response" including C-type lectin, pathogen and heat categories (Fig 2E). In addition, Gene Ontology (GO) term enrichment analysis of module red genes further highlighted the enrichment for the terms "Immune system process" and "Response to biotic stimulus" (S1B Fig).

Recently, *Ghaddar et al.* presented a gene expression atlas of adult *C. elegans* with single-cell RNA sequencing [19]. They categorized the intestinal cells into multiple subtypes: intestine anterior (two), intestine middle and intestine posterior (two). To place our findings in the context of previously defined intestinal cell subtypes, we compared the results of our datasets to theirs. INT1 enriched genes were upregulated in the anterior intestine cluster relative to other intestinal subtypes, supporting our conclusion that INT1 represents a translationally distinct intestinal subset (S1C Fig).

Next, we decided to characterize the translatomic differences between INT1 and INT2-9 cells. We began with the differentially expressed genes in INT1 cells relative to INT2-9 cells in the fed state. There were 153 upregulated and 58 downregulated genes (Fig 2F), and we found *ins-7* among the upregulated genes, consistent with our prior report of its restricted expression in INT1 [6]. To identify the categories of the differentially expressed genes in INT1 cells under the fed condition, we performed WormCat category enrichment analysis and also used ShinyGO [20] to conduct Gene Ontology (GO) term enrichment analysis with a hierarchical clustering tree, allowing us to visualize the overlapping relationships among enriched GO terms. In the upregulated genes with WormCat analysis, we found genes involved in "Stress Response" including pathogen, C-type lectin, and heat-shock categories (Fig 2G). Further, the results from ShinyGO demonstrated a cluster of GO terms related to "Immune Response" and "Unfolded Protein Response" (Fig 2H). In contrast, no functional enrichment was detected among the INT1-downregulated genes. Together,

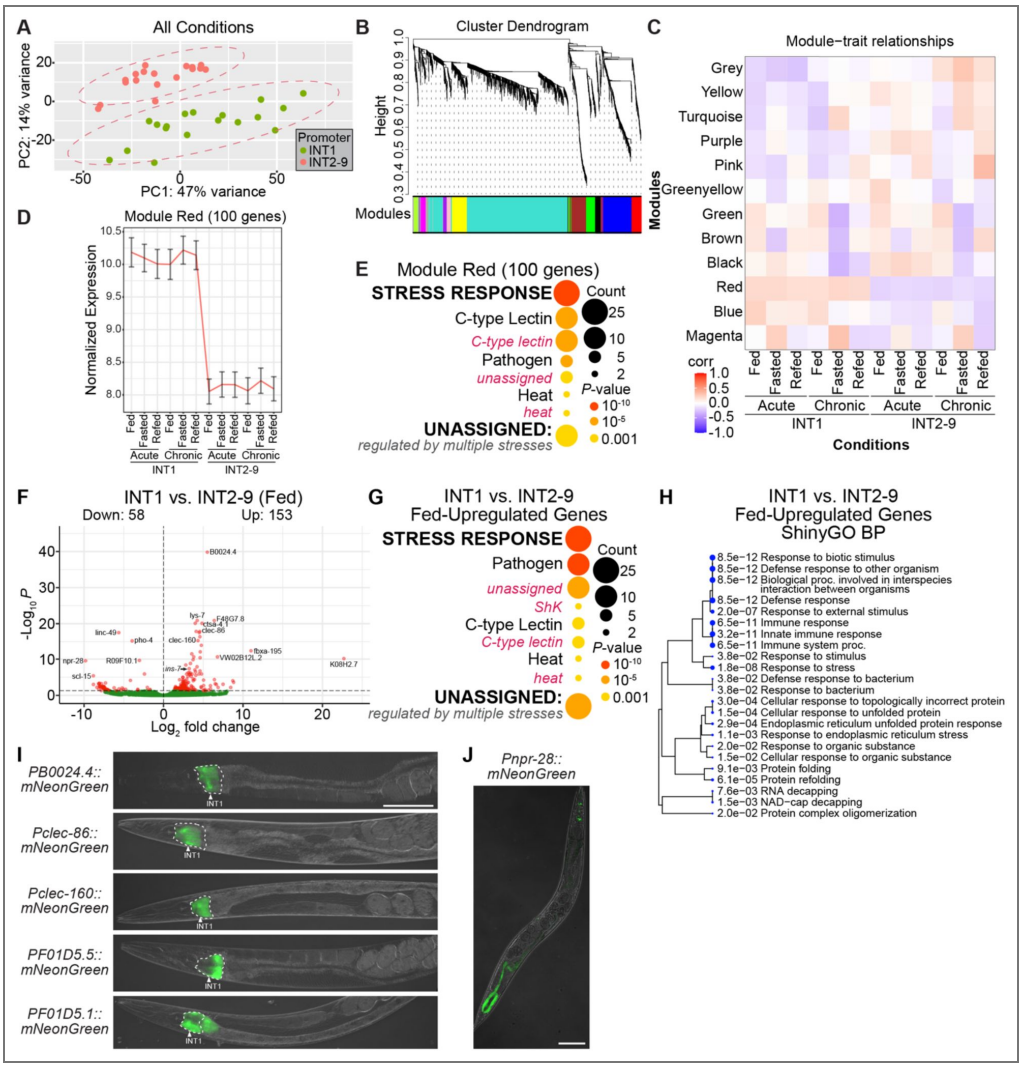

Fig 2. Identification of the fundamental differences between INT1 and INT2-9 translatomes.

(A) Principal component analysis showing translatomic variability across the first two principle components of TRAP-Seq data from INT1 and INT2-9 promoters under both acute and chronic conditions (fed, fasted, and refed). Ellipse was computed using the mean and covariance of PC1 and PC2 for each line. (B) Cluster dendrogram produced by average linkage hierarchical clustering in WGCNA. The color row under the dendrogram indicates the module assignment. (C) Pearsons correlations of TRAP-seq conditions with WGCNA modules. Each row represents a WGCNA module and its means correlation to the indicated trait across replicates.The color of each cell indicates the mean pearsons correlation coefficient between the module and the condition; red represents a positive correlation and blue represents a negative correlation. (D) Average expression of red modules genes in the TRAP-seq conditions. The y-axis shows mean variance stabilized expression across all genes and replicates per condition with standard deviation indicated by the error bars. (E) WormCat visualization of categories enriched in genes of module red. Categories 1 are all bold uppercase; Categories 2 are capitalized; Categories 3 are gray italics. The size of the bubbles indicates the gene counts in the category and the color of the bubble represents the adjusted p-value. (F) Volcano plot of differentially expressed genes for INT1 fed versus INT2-9 fed. High confidence differentially expressed genes are labeled. The horizontal dashed line indicates an adjusted p-value cutoff of 0.05. (G) WormCat visualization of categories enriched in genes upregulated in INT1 cells versus INT2-9 cells in the fed state. Categories 1 are all bold uppercase; Categories 2 are capitalized; Categories 3 are gray italics. The size of the bubbles indicates the gene counts in the category and the color of the bubble represents the adjusted p-value. (H) A hierarchical clustering tree of significantly enriched GO terms (Biological Process, BP) in the upregulated genes for INT1 fed versus INT2-9 fed by ShinyGO. GO terms with many shared genes are clustered together. Larger dots indicate more significant adjusted p-values. (I) Fluorescent images of transgenic animals bearing *PB0024.4::mNeonGreen*, *Pclec-86::mNeonGreen*, *Pclec-160::mNeonGreen*, *PF01D5.5::mNeonGreen* or *PF01D5.1::mNeonGreen* transgenes. The white arrowhead indicates *mNeonGreen* expression in INT1 cells. Scale bar, 100 μm. (J) Fluorescent image of a transgenic animal bearing *Pnpr-28::mNeonGreen* transgene. Scale bar, 100 μm.

these findings show that INT1 cells are characterized by a stress- and immune-responsive translational program in the fed state, marking a strong and clear distinction from the rest of the intestine.

C-type lectins and ShKT domain-containing proteins are enriched in INT1 cells

We noticed that many INT1-differentially expressed genes were not assigned to a category by WormCat or annotated by ShinyGO. To further explore their molecular functions, we used the InterPro database to annotate the protein domains for each gene and assign the domains into several main categories, such as “Enzyme”, “Membrane Protein”, and “Transcription Factor”. Genes encoding domains that did not fall into these categories, as well as those lacking identifiable domains, were grouped as “Genes with Unknown Functions” (S2A and S2B Fig). Among the 149 upregulated genes in INT1, we found 11 encoding C-type lectins (S2A Fig). C-type-lectin-domain-containing proteins are notable for pathogen recognition and the initiation of immune responses in vertebrates [21]. In *C. elegans*, the expression of many distinct C-type lectins has previously been found to be induced in a pathogen-specific exposure [22, 23].

In addition, we discovered a subset of INT1 upregulated genes encoding ShKT domains within the genes with unknown functions (S2A Fig). The ShK toxin (ShKT) is a potassium (K^+) channel blocker originally isolated from the sea anemone *Stichodactyla helianthus* [24]. ShKT domain-containing proteins have been reported in parasitic nematode secretomes [25] and shown to modulate the activity of human effector memory T cells by blocking voltage-gated potassium channels [26]. Their biological functions in *C. elegans*, however, remain unclear. Our findings that specific ShKT domain-containing proteins are specifically expressed in INT1 cells are intriguing. Notably, several INT1-upregulated ShKT proteins, including F01D5.1, F01D5.5 and SYSM-1, were previously found to be upregulated by PMK-1 (p38 MAPK) [27], a key regulator of pathogen-induced immune responses in *C. elegans* [27, 28], suggesting that these ShKT proteins may contribute to intestinal immune functions.

To validate our TRAP-Seq findings and define the spatial expression of INT1-enriched genes, we chose key candidate genes with high fold change and low adjusted p-value (therefore, the most significantly altered genes, Fig 2I and S1D-H Fig) to generate transcriptional reporters using their endogenous promoters and 3’UTRs. We started with *B0024.4*, a membrane raft protein-coding gene with the lowest adjusted p-value in the INT1-enriched genes, which revealed tight expression restricted to INT1 cells. We next decided to examine reporters for two C-type lectin genes, *clec-86* and *clec-160*, and two ShKT protein-coding genes, *F01D5.1* and *F01D5.5*. Reporters for *clec-86*, *clec-160* and *F01D5.5* also exhibited highly specific expression in INT1, whereas *F01D5.1* was expressed in both INT1 and INT2. Out of curiosity, we also generated a reporter line for the most highly downregulated gene *npr-28* in INT1, and interestingly, found that it was restricted to the posterior intestinal cells INT7-9, with no expression in the anterior intestine (Fig 2J). Collectively, these analyses corroborate the spatial restriction of our TRAP-Seq method and demonstrate that INT1-upregulated and INT1-downregulated genes exhibit distinct spatial expression patterns along the intestine.

Comparisons of enriched categories under acute and chronic conditions identify ShKT domain-containing proteins as stable INT1-specific markers

We next wished to evaluate whether there are specific differences between INT1 and INT2-9 cells under acute fasting and refeeding. In the acute fasted state, INT1 displayed 90 upregulated and 12 downregulated genes (Fig 3A). WormCat analysis of upregulated genes revealed those involved in “Stress Response” including C-type lectin and pathogen categories (Fig 3B), while ShinyGO identified a cluster of GO terms related to “Defense Response” (Fig 3C). In the acute refed state, we observed 52 INT1-upregulated and 35 INT1-downregulated genes (Fig 3D). Enriched categories of the upregulated genes again included “Stress Response”, particularly pathogen and C-

type lectins by WormCat (Fig 3E), with GO terms related to "Defense Response" and "Immune Response" by ShinyGO (Fig 3F). InterPro annotations of INT1-upregulated genes revealed consistent representation of "Enzyme", "C-type Lectin" and "Membrane Protein" categories across fed, acute fasted, and acute refed states (S3A and S3C Fig). Although enriched functional categories were similar between the 2 intestinal sub-compartments, a Venn diagram analysis of the "Stress Response" genes demonstrated only partial overlap across states (Fig. 4A), suggesting that translational differences between INT1 and INT2-9 vary depending on physiological states.

To further test this possibility, we compared gene lists from 4 major InterPro categories ("Enzyme", "Membrane Protein", "C-type Lectin" and "ShKT Protein") across fed, acute fasted and acute refed states (Fig 4B-H). While "Enzyme", "Membrane Protein", and "C-type Lectin" categories exhibited only partial overlap, the "ShKT Protein" category showed near-complete overlap across conditions (Fig 4E), suggesting that ShKT proteins represent stable INT1-specific markers under acute conditions.

We next extended our analysis to chronic fasting and refeeding, which elicit more pronounced metabolic shifts in the intestine. In the chronic fasted state, INT1 exhibited 111 upregulated and 77 downregulated genes (Fig 3G). WormCat analysis of the upregulated genes again identified enrichment for "Stress Response" categories, including C-type lectins and pathogen-related genes (Fig 3H), while ShinyGO revealed a cluster of GO terms related to "Immune Response" (Fig 3I). Similar enrichments were observed in the chronic refed state (Fig 3K and 3L). InterPro annotations of INT1 upregulated genes revealed categories consistent with acute conditions, including "Enzyme", "Membrane Protein" and "C-type Lectin" (S4A and S4C Fig). Comparison of gene lists demonstrated partial overlap within these categories (Fig 4J-L, 4N-P). Strikingly, however, upregulated ShKT genes showed near-complete overlap across chronic conditions (Fig 4M).

Finally, we compared the INT1-upregulated ShKT genes across both acute and chronic conditions. Venn diagram analysis revealed complete overlap, with the same set of 11 ShKT genes consistently upregulated in all conditions (Fig 4R). These findings demonstrate that ShKT domain-containing proteins represent robust INT1-specific markers, stable across both acute and chronic states. Thus, pathogen-sensing, detoxification and mounting an organismal response to incoming information from the gut lumen are the principal functions of INT1.

INT1 and INT2-9 cells exhibit distinct fasting and refeeding responses under acute and chronic conditions

Given the fundamentally distinct translatomes of the INT1 and INT2-9 cells, we next investigated whether these differences extend to their responses to fasting and refeeding. Specifically, we sought to determine if the translatomic profiles of INT1 and INT2-9 cells exhibit distinct regulatory patterns in response to metabolic shifts induced by fasting and subsequent refeeding. Looking at the concordance of differentially expressed genes during chronic and acute fasting between INT1 and INT2-9 cells, we identified fasting-response genes with opposing regulation between the two intestinal subsets (Fig 5A and 5B). For instance, 270 genes were upregulated in INT1 following acute fasting but downregulated in INT2-9 under the same condition (Fig 5A), indicating divergent translational responses to metabolic shifts.

We next listed all differentially expressed genes (DEGs) in INT1 and INT2-9 under acute and chronic conditions. Overall, INT1 exhibited fewer DEGs than INT2-9 (Fig 5C). To rule out the possibility that INT1 DEGs represented a subset of INT2-9 DEGs, we used Venn diagrams to compare all the INT1 and INT2-9 DEGs from both acute and chronic conditions (Fig 5D). We found two major features of these fasting and refeeding response genes. Notably, INT1 DEGs were not a subset of INT2-9 DEGs regardless of acute or chronic conditions, but rather represented distinct gene sets (Fig 5D). Another key distinction is that for both INT1 and INT2-9, the acute response genes did not overlap substantially with chronic response genes, indicating that distinct translational programs are engaged during acute versus chronic conditions (Fig 5D).

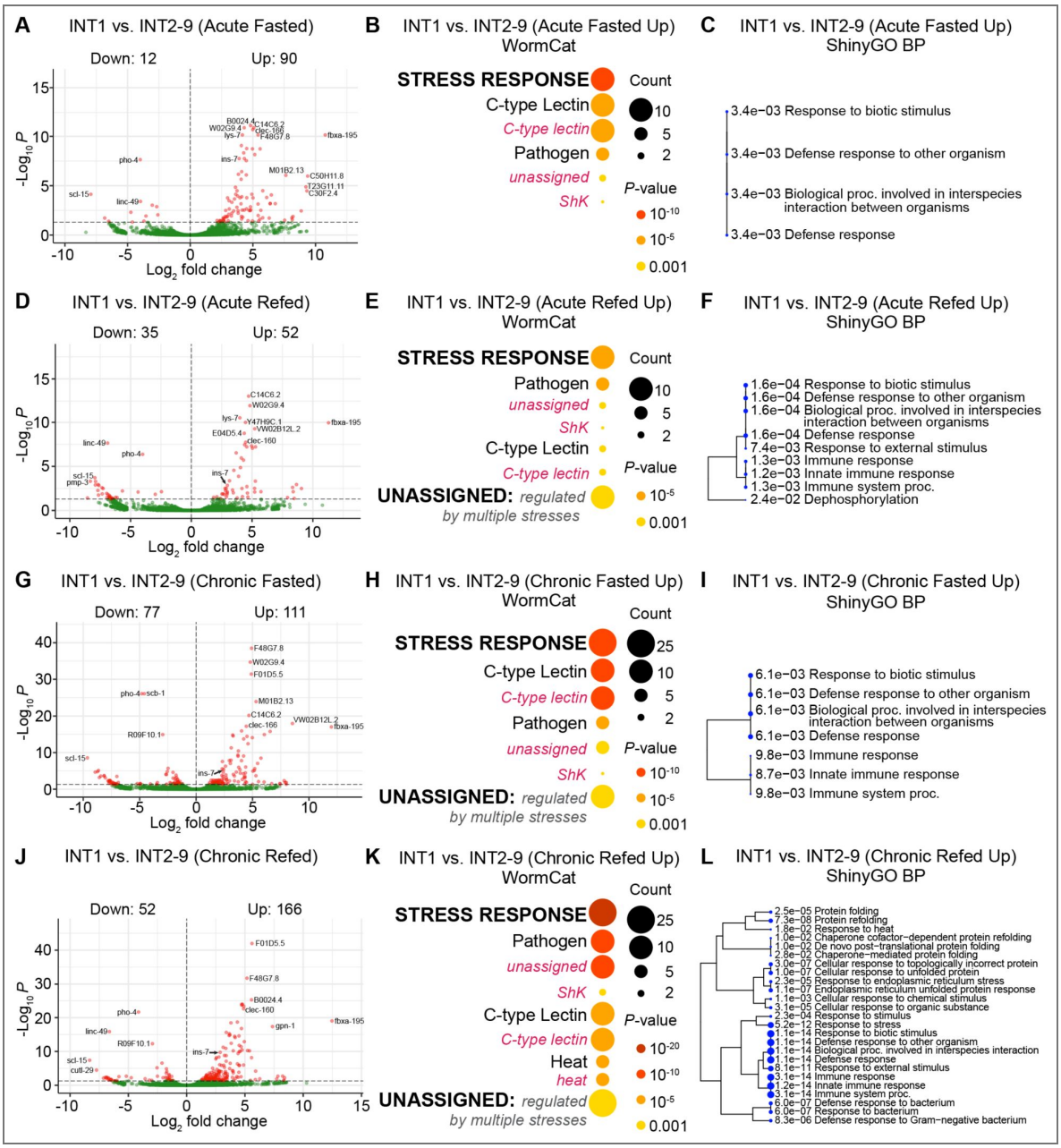

Fig 3. Identification of the differences between INT1 and INT2-9 translatomes under acute and chronic conditions.

(A, D, G, J) Volcano plot of differentially expressed genes for INT1 versus INT2-9 in acute fasted, acute refed, chronic fasted and chronic refed states. High confidence differentially expressed genes. The horizontal dashed line indicates an adjusted p-value cutoff of 0.05. (B, E, H, K) WormCat visualization of categories enriched in genes upregulated in INT1 cells versus INT2-9 cells in acute fasted, acute refed, chronic fasted and chronic refed states. Categories 1 are all bold uppercase; Categories 2 are capitalized; Categories 3 are gray italics. The size of the bubbles indicates the gene counts in the category and the color of the bubble represents the adjusted p-value. (C, F, I, L) A hierarchical clustering tree of significantly enriched GO terms (Biological Process, BP) in the upregulated genes for INT1 versus INT2-9 in acute fasted, acute refed, chronic fasted and chronic refed states by ShinyGO. GO terms with many shared genes are clustered together. Larger dots indicate more significant adjusted p-values.

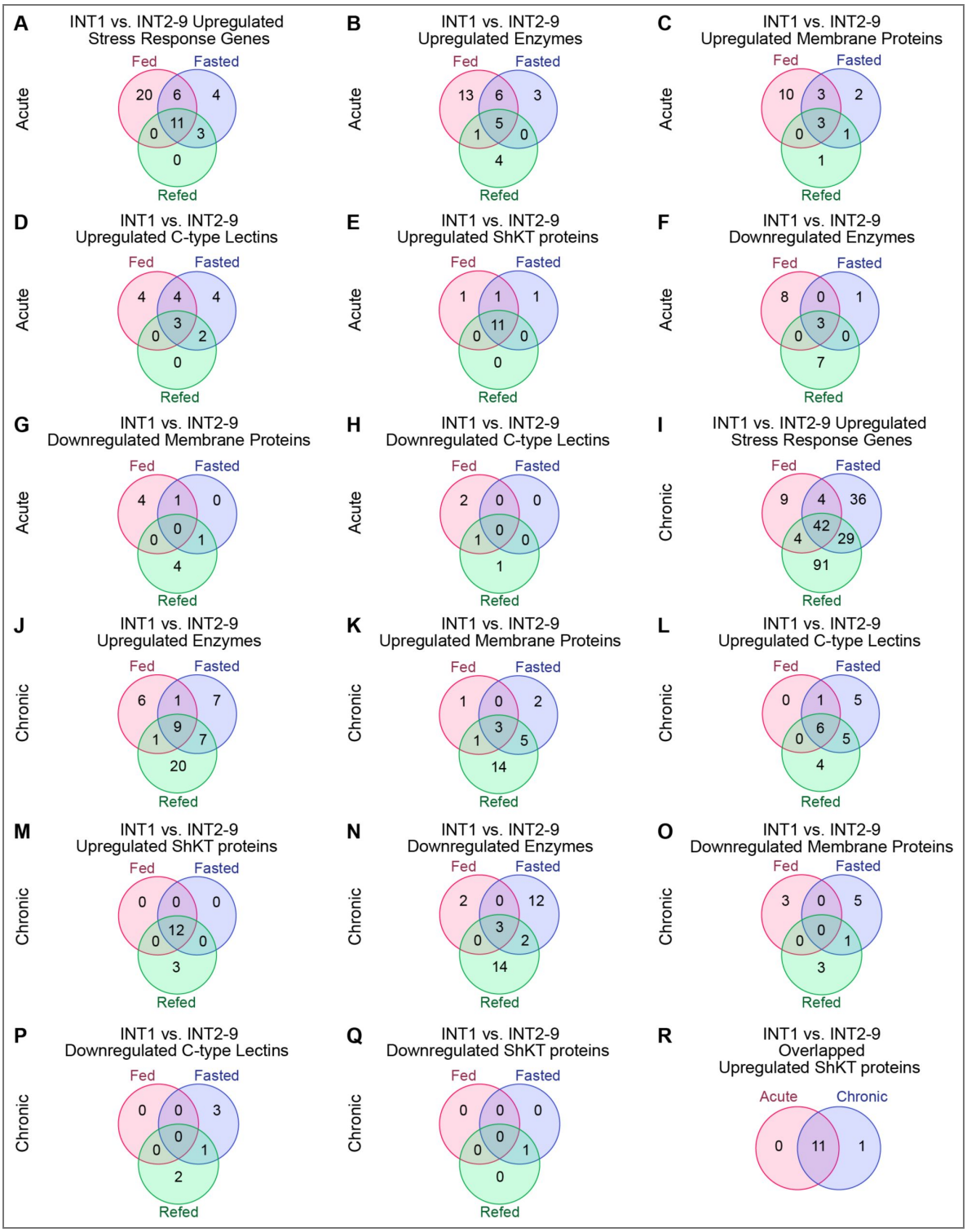

Fig 4. Comparisons of InterPro categories for INT1 versus INT2-9 under acute and chronic conditions.

(A-H) Venn diagrams showing the number of upregulated or downregulated genes in specific categories for INT1 versus INT2-9 under the three acute conditions (fed, fasted, and refed). (I-Q) Venn diagrams showing the number of genes in specific categories for INT1 versus INT2-9 under the three chronic conditions (fed, fasted, and refed). (R) Venn diagram showing the overlap between overlapped upregulated ShKT proteins for INT1 versus INT2-9 under acute and chronic conditions.

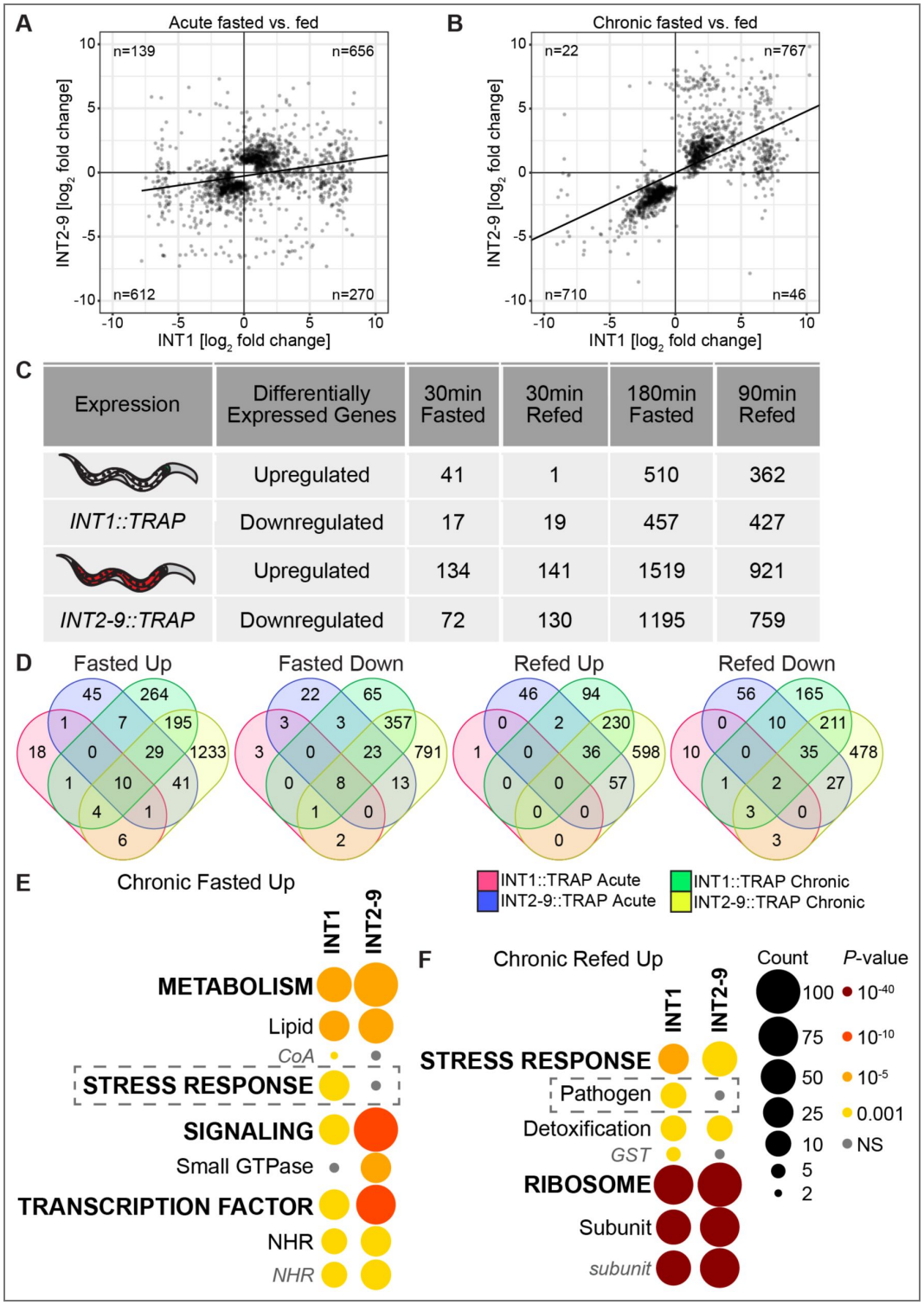

Fig 5. Comparison of fasting and refeeding responses between INT1 and INT2-9 cells under acute and chronic conditions.

(A, B) Scatterplots comparing the acute and chronic fasting response genes in INT1 vs INT2-9 differential expression. The top 1000 DEGs by significance were selected for each line and fasting response to be compared, with a regression line fitted to compared INT1 vs INT2-9 response. (C) Table of differentially expressed genes (FDR < 0.05) under acute and chronic conditions for INT1 and INT2-9 datasets. (D) Venn diagrams showing the number of differentially expressed genes (FDR < 0.05) in fasting and refeeding conditions for INT1 and INT2-9 datasets. (E, F) WormCat visualization of categories enriched in upregulated genes in INT1 cells and INT2-9 cells under chronic fasting or refeeding conditions. Categories 1 are all bold uppercase; Categories 2 are capitalized; Categories 3 are gray italics. The size of the bubbles indicates the gene counts in the category and the color of the bubble represents the adjusted p-value. (E) is part of S6A Fig, and (F) is part of S7A Fig.

To identify the enriched categories of these INT1 and INT2-9 DEGs under each condition, we performed WormCat analysis and found that INT1 datasets generally had fewer enriched categories than INT2-9 datasets under each condition. (S5A and S5B Fig, S6A and S6B Fig). In the acute fasted state, upregulated genes in both INT1 and INT2-9 were enriched for "Metabolism", whereas categories including "Stress Response", "Transcription Factor", and "Lysosome" were specific to INT2-9 (S5A Fig). Among the downregulated genes in both cell types in the acute fasted state, we found genes involved in "Ribosome", including ribosomal subunit genes (S5B Fig). Interestingly, in the acute refed state, genes involved in "Ribosome" were upregulated in INT2-9 (S5C Fig), suggesting the sensitivity of ribosomal gene expression to acute fasting and refeeding. Additional categories, such as "Transcription Factor" and "Proteolysis Proteasome", were enriched exclusively among INT2-9 downregulated genes in the acute refed state (S5D Fig).

Further, we observed that chronic conditions elicited broader and more diverse enrichment patterns than acute states in both INT1 and INT2-9 (S5, S6 and S7 Figs). Although this is an expected result, the category term "Stress Response" was surprisingly enriched only among INT1-upregulated genes in the chronic fasted state (Fig 5E), whereas "Pathogen" was uniquely enriched among INT1-upregulated genes in the chronic refed state (Fig 5F), underscoring an important potential specialization of INT1 in stress and immune responses. Conversely, both INT1 and INT2-9 datasets shared enrichment for "Ribosome" and "Metabolism" among downregulated genes in the chronic fasted state and upregulated genes in the chronic refed state (S6B and S7A Figs), suggesting that protein translation and metabolic regulation are highly responsive to chronic fasting and refeeding.

Taken together, these results demonstrate that INT1 and INT2-9 cells engage distinct translational programs during fasting and refeeding. The divergence is particularly evident under chronic conditions, where INT1 uniquely activates stress- and pathogen-related programs, suggesting specialized roles for INT1 in maintaining homeostasis under chronic conditions. However, because a large portion of the INT1 DEGs remain unassigned by WormCat, the full extent of INT1-specific regulatory programs may not be fully captured by gene set enrichment analyses.

INT1 cells modulate pathogen avoidance, survival, and peptide secretion

To begin to annotate and assign functions to the genes emerging from our datasets, we examined the pathogen response and peptide secretion functions of the INT1 cells, and the roles of the most highly regulated genes therein. To study pathogen response, we noted that previous studies had implicated INT1-enriched genes in immune responses. For example, expression of *B0024.4* is induced upon exposure to pathogenic *S. maltophilia* JV3 strain [29], and *clec-42*, one of our INT1-upregulated genes, is exclusively expressed in INT1 at all larval stages and mediates resistance to pathogen Bt247 [23]. To test whether INT1-upregulated genes contribute to immune responses, we used an INT1-specific RNAi strain (*sid-1; Pges-1ΔB::sid-1*) to knock down *clec-86* and *clec-160*, and then performed PA14 avoidance and PA14 slow-killing assays [30]. Interestingly, animals with INT1-specific knockdown of either gene exhibited impaired PA14 avoidance (Fig 6A and 6B) and significantly increased survival on PA14 (Fig 6C). These findings suggest that INT1 cells execute specialized, gene-dependent immune functions during pathogen exposure.

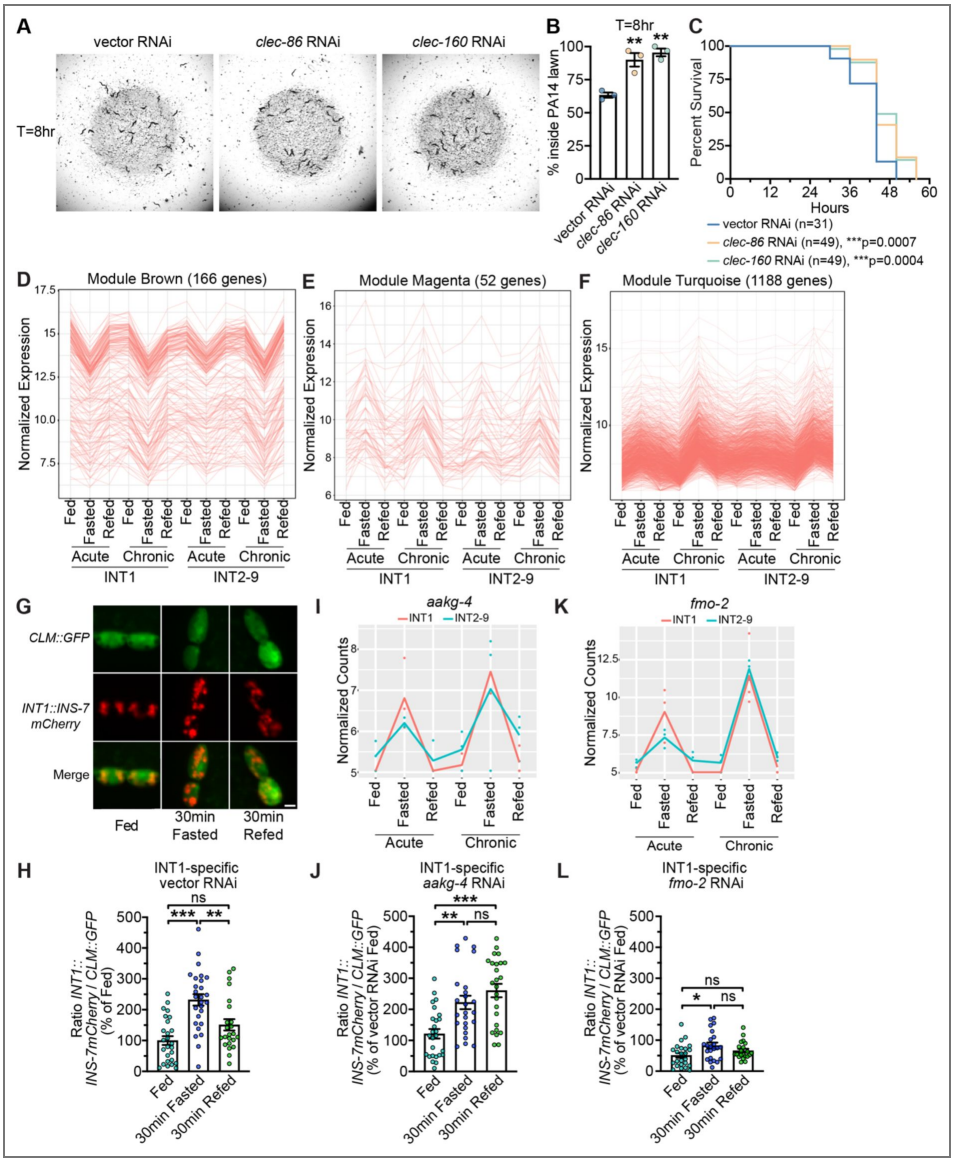

Fig 6. INT1-specific genes modulate behavior and metabolism.

(A) The vector, *clec-86*, and *clec-160* RNAi treated *sid-1;INT1::sid-1* animals after 8 hr exposure to PA14 lawns are shown. (B) The distribution of indicated RNAi-treated *sid-1;INT1::sid-1* animals at hour 8 after being transferred to PA14 plates. At hour 0, a total of 30 animals were placed near the PA14 lawn. Data are expressed as a percentage of the animals staying inside PA14 lawn at hour 8 ± SEM (n=3, 3 plates per RNAi treatment, 30 animals on each plate). **p<0.01 by one-way ANOVA (Dunnett). (C) The lifespan of each indicated RNAi-treated animal after being transferred to PA14 lawn was determined by counting the number of live and dead animals every 6hr until all animals had died. Data are plotted as the percentage of animals that survived on any given hour relative to the number of live animals at hour 0. The number of animals for each RNAi treatment is indicated in the figure panels. ***p<0.001 by Log-rank Test. The median survival is 44 hours for all the RNAi treatments. (D-F) Average expression of brown, magenta, and turquoise modules genes in the TRAP-seq conditions. The y-axis shows mean variance stabilized expression across all genes and replicates per condition and module with standard deviation indicated by the error bars. (G) Representative images of *sid-1;INT1::sid-1* animals bearing integrated *INT1::INS-7mCherry* and *CLM::GFP* transgenes treated with vector RNAi at the indicated time points. Scale bar, 5 μm. (H, J, L) *sid-1;INT1::sid-1* animals bearing integrated *INT1::INS-7mCherry* and *CLM::GFP* transgenes were treated with vector, *aakg-4* or *fmo-2* RNAi. INS-7 secretion levels were measured after 30 min fasting and after 30 min refeeding. The intensity of INS-7mCherry fluorescence within a single coelomocyte was quantified and normalized to the area of CLM::GFP expression for each RNAi treatment. Data are expressed as a percentage of the normalized INS-7mCherry fluorescence intensity of fed animals treated with vector RNAi ± SEM (n=21-27). *p<0.05, **p<0.01, ***p<0.001, ^{ns}p>0.05 by one-way ANOVA (Dunnett T3). (I, K) Normalized expression plots of *aakg-4* and *fmo-2* under all conditions in INT1 and INT2-9 cells by replicate.

From the WGCNA, we noted that some modules (brown, magenta, turquoise) contained genes with an undulating change in expression levels in response to fasting and refeeding under both acute and chronic conditions (Fig 6D-F). These genes could be classified as "fasted up/refed down" or "fasted down/refed up". WormCat analysis of brown module genes identified enrichment for "Ribosome" and "Metabolism", consistent with categories previously linked to ribosomal subunit genes (S6B, S7A, and S8A Figs). Notably, modules magenta and turquoise contained "fasted up/refed down" genes. To determine the strength of the induction across lines we used a Wilcoxan test comparing the distribution of the normalized expression of module genes between fed and fasted conditions. We found the induction in INT2-9 cells (p = 5.6e-4, average LFC = 0.07) after acute fasting was weaker in the turquoise module when compared to INT1 cells (p = 5.6e-50, average LFC = 0.12), suggesting these undulating genes were more INT1-specific (Fig 6E and 6F).

Given our prior finding that the gut peptide INS-7 is secreted from INT1 cells in response to acute fasting [6], we next investigated whether INT1-specific undulating genes could modulate this response. Using the INT1-specific RNAi strain (*sid-1; Pges-1ΔB::sid-1*) crossed into an INS-7 secretion reporter, we confirmed that vector RNAi-treated animals displayed the expected undulating INS-7 secretion levels upon acute fasting and refeeding (Fig 6G and 6H), as previously described [6]. We next targeted two INT1-specific undulating genes, *aakg-4* and *fmo-2*, which showed the largest absolute fold changes across acute fasting and refeeding for INT1-specific RNAi (Fig 6I and 6K). *aakg-4* is the gene encoding one of the five ψ subunits of the AMP-activated protein kinase (AMPK) in *C. elegans* [31]. However, the physiological role of *aakg-4* in the intestine is unknown. Remarkably, INT1-specific *aakg-4* knockdown prevented INS-7 secretion from returning to basal levels after refeeding, indicating a requirement for *aakg-4* in resetting INS-7 secretion and suggesting that INS-7 release from INT1 cells is subject to energy-dependent regulation, consistent with its modulation by fasting and refeeding (Fig 6J). The second gene *fmo-2*, encoding flavin-containing monooxygenase-2, is known to promote longevity under hypoxia and dietary restriction [32]. FMOs contain the prosthetic group that binds FAD^+ and utilize the cofactor NADPH together with O_2 to catalyze substrate oxygenation, generating $NADP^+$ as a by-product [33]. Animals subjected to INT1-specific *fmo-2* knockdown displayed a normal fasting-induced INS-7 secretion, but exhibited reduced basal INS-7 secretion and impaired refeeding response (Fig 6L). Given that NADPH/$NADP^+$ ratio is a central determinant of cellular redox state and energy metabolism [34], this result further supports the notion that regulation of INS-7 secretion in INT1 cells is coupled to energy-sensing metabolic pathways.

Together, these results demonstrate that INT1 cells integrate immune and metabolic cues. By regulating pathogen avoidance and survival through lectin genes and modulating INS-7 secretion via energy-responsive genes such as *aakg-4* and *fmo-2*, INT1 cells function as a specialized intestinal subset that senses energy states and coordinates gut peptide secretion to maintain organismal homeostasis.

Pyruvate is crucial for regulating INS-7 peptide secretion from INT1 cells

We were intrigued by the findings with *aakg-4* and *fmo-2*, which suggested that cellular energy status may govern the refeeding response of INS-7 secretion. Notably, the effect does not appear to be mediated by changes in intestinal fat content, as lipid levels remain unaltered during acute fasting and refeeding (Fig 1B and 1C). These observations led us to hypothesize that INT1 cells may integrate specific sensory cues to reset INS-7 secretion in response to food availability. To explore this possibility, we first evaluated the contribution of mechanosensory inputs. Fasted worms refed with 0.5 μm latex beads, comparable in size to *E. coli* [35, 36], failed to restore INS-7 secretion to basal levels, whereas refeeding with OP50 fully normalized INS-7 secretion (Fig 7A), suggesting that mechano-stimulus alone was not sufficient to induce the refeeding response of INS-7 secretion. Because *C. elegans* can detect secreted molecules from bacteria and trigger a stress response [37], we next exposed fasted animals to cell-free OP50 culture supernatant [37, 38]. Supernatant alone likewise failed to reset INS-7 secretion (Fig 7A). A combination of beads and

supernatant was similarly ineffective (Fig 7A). In contrast, UV-killed OP50 completely reinstated basal INS-7 secretion (Fig 7A), indicating that chemicals or nutrients from bacteria, rather than mechano-stimulus or secreted molecules, mediate the refeeding response.

Next, we set out to pinpoint the bacterial nutrient or chemical most critical for regulating INS-7 secretion during refeeding. Based on the requirement of *aakg-4* and *fmo-2* for INS-7 secretion dynamics, we tested whether restoring cellular energy states after fasting could return INS-7 secretion to baseline. Glucose serves as a primary cellular energy source, undergoing glycolysis to generate pyruvate, which in turn fuels downstream metabolic pathways to produce energy. However, refeeding fasted worms with 2% glucose, a concentration considered a high-glucose diet for *C. elegans* [47], failed to normalize INS-7 secretion, which remained elevated (Fig 7B). In contrast, remarkably, refeeding with 100 mM pyruvate, a dose effective in prior studies [47], fully recapitulated the refeeding response observed with OP50 (Fig 7B). This effect was dose-dependent (S9A Fig). Thus, pyruvate, a key molecule derived from glycolysis and a precursor metabolite for numerous biochemical processes, is sufficient to substitute for bacterial food in restoring INS-7 secretion to baseline after fasting.

After entering the cell, pyruvate can be converted to lactate or alanine in the cytosol or transported into the mitochondrial matrix via the mitochondrial pyruvate carrier (MPC) [39, 40] to enter the citric acid cycle, which generates energy [41]. INT1-specific RNAi of the two *C. elegans* MPC genes (*mpc-1* and *mpc-2*) abolished the pyruvate-induced restoration of INS-7 secretion (Fig 7C and 7D), demonstrating that mitochondrial import of pyruvate is required. Within the matrix, pyruvate is converted to acetyl-CoA by pyruvate dehydrogenase (*pdha-1* and *pdhb-1* in *C. elegans*) or to oxaloacetate by pyruvate carboxylase (*pyc-1* in *C. elegans*). INT1-specific knockdown of either pathway suppressed fasting-induced INS-7 secretion and abolished secretion dynamics (Fig 7E and 7F). Since chronic *pdha-1* and *pdhb-1* knockdown lowered basal INS-7 secretion level, we acutely inhibited pyruvate dehydrogenase during refeeding with the specific inhibitor 3-fluropyruvate (3-FP); this intervention prevented INS-7 secretion from returning to basal levels (S9B Fig), suggesting that the conversion of pyruvate to acetyl-CoA is required for the refeeding response of INS-7 secretion.

If intracellular pyruvate is the crucial determinant of INS-7 secretion, we predicted that maintaining pyruvate levels in the INT1 cells during fasting should suppress the fasting-induced INS-7 secretion. Indeed, worms fasted on NGM agar supplemented with 100 mM pyruvate showed no induction of INS-7 secretion (Fig 7G), suggesting pyruvate alone is sufficient to suppress fasting-induced INS-7 secretion. Collectively, these findings identify mitochondrial pyruvate metabolism as the key signal sensed by INT1 enteroendocrine cells to couple nutritional availability with the fluctuation in INS-7 peptide secretion during fasting and refeeding.

Discussion

In the human intestine, both epithelial and immune cell compositions shift dramatically along the anterior-posterior axis, with region-specific cellular neighborhoods for epithelial, stromal, and immune cells contributing to distinct physiological functions [42]. In contrast, the *C. elegans* intestine comprises only 20 epithelial cells and lacks resident immune cells, raising the question of whether spatially defined molecular and functional heterogeneity also exists in this simplified but powerful model system. Our findings, together with prior observations, support the view that *C. elegans* intestinal subsets are molecularly and functionally distinct. The data show that the most pronounced difference between INT1 and the rest of the intestine at the RNAseq level, is the expression of stress response genes in INT1. Although there are some nuanced differences, the prevalence of stress response genes persists across feeding and fasting conditions. This difference, combined with the evidence that INT1 cells secrete the enteroendocrine peptide INS-7 [6] (Fig 6) is strongly reminiscent of the mammalian enteroendocrine cells, which also secrete peptides and show strong expression of stress response genes [43, 44]. We suggest that this category term reflects not only a canonical stress response, but also a broader response to shifts in the luminal

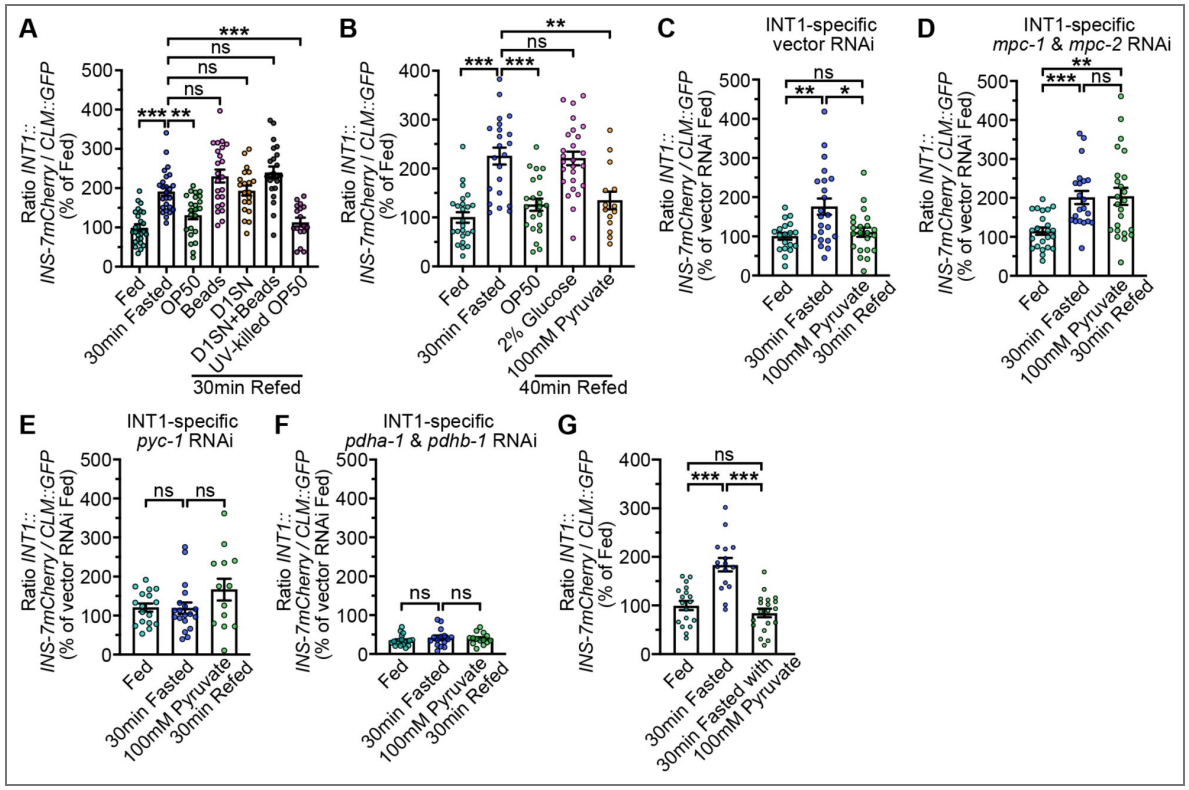

Fig. 7. Pyruvate is critical for maintaining INS-7 secretion dynamics in INT1 cells.

(A) INS-7 secretion dynamics during fasting and re-feeding with OP50, latex beads, Day 1 OP50 supernatant (D1SN), Day 1 OP50 supernatant with latex beads (D1SN+Beads), and UV-killed OP50 were determined at the indicated time points. The intensity of INS-7mCherry fluorescence within a single coelomocyte was quantified and normalized to the area of CLM::GFP expression for each time point. Data are expressed as a percentage of the normalized INS-7mCherry fluorescence intensity of wild-type fed animals ± SEM (n=20-26). **p<0.01, ***p<0.001, ^{ns}p>0.05 by one-way ANOVA (Dunnett T3). (B) INS-7 secretion dynamics during fasting and re-feeding with OP50, 2% glucose and 100 mM pyruvate were determined at the indicated time points. The intensity of INS-7mCherry fluorescence within a single coelomocyte was quantified and normalized to the area of CLM::GFP expression for each time point. Data are expressed as a percentage of the normalized INS-7mCherry fluorescence intensity of wild-type fed animals ± SEM (n=14-26). **p<0.01, ***p<0.001, ^{ns}p>0.05 by one-way ANOVA (Dunnett T3). (C-F) INS-7 secretion dynamics in INT1-specific vector RNAi, *mpc-1* and *mpc-2* RNAi, *pyc-1* RNAi, *pdha-1* and *pdhb-1* RNAi-treated animals during fasting and re-feeding with 100 mM pyruvate were determined at the indicated time points. The intensity of INS-7mCherry fluorescence within a single coelomocyte was quantified and normalized to the area of CLM::GFP expression for each time point. Data are expressed as a percentage of the normalized INS-7mCherry fluorescence intensity of vector RNAi fed animals ± SEM (n=13-24). *p<0.05, **p<0.01, ***p<0.001, ^{ns}p>0.05 by one-way ANOVA (Dunnett T3). (G) INS-7 secretion dynamics during fasting and fasting with the presence of 100 mM pyruvate were determined at the indicated time points. The intensity of INS-7mCherry fluorescence within a single coelomocyte was quantified and normalized to the area of CLM::GFP expression for each time point. Data are expressed as a percentage of the normalized INS-7mCherry fluorescence intensity of fed animals ± SEM (n=16-19). ***p<0.001, ^{ns}p>0.05 by one-way ANOVA (Dunnett T3).

environment, which INT1 cells are anatomically poised to detect well before the absorption of nutrients has begun further down the intestine (INT2-9). Thus, we believe INT1 cells are a newly defined enteroendocrine cell-type within the *C. elegans* intestine.

In the present study, we utilized INT1- and INT2-9-specific promoters to perform TRAP-Seq analyses under fasting and refeeding conditions. While comparisons between INT1 and INT2-9 cells revealed marked differences, this approach likely underrepresents heterogeneity among the INT2-9 cells themselves. Prior studies demonstrated that posterior intestinal cells initiate the rhythmic defecation motor program [45, 46], and our dataset identified *npr-28*, which is specifically expressed in the posterior intestinal cells INT7-9 (Fig 2J), further underscoring molecular diversity across intestinal segments. Future identification of promoters with more restricted expression within the INT2-9 subset will be crucial for functionally resolving the spatial map of the *C. elegans* intestine.

We previously identified INT1 as enteroendocrine cells that secrete the gut peptide INS-7 preferentially during acute food withdrawal to suppress neuronally stimulated fat loss [6]. Additional lines of evidence also point to the specialization of the anterior-most INT1 cells. First, acid phosphatase staining for intestinal brush border could not be detected in INT1 cells [15, 47]. Second, Methyl red staining showed strong red staining of acidic vacuoles in INT1 cells. From INT2 to INT9 cells, vacuoles were stained gradually from orange-yellow (neutral-alkaline) to yellow (alkaline) with methyl red [47], suggesting the pH of intracellular vacuoles is lower in INT1 cells. Third, ultrastructural analysis highlighted enrichment of rough ER, Golgi, and mitochondria in INT1, consistent with a secretory function, whereas INT2-9 cells preferentially accumulate yolk and lipid vacuoles for storage [48]. Fourth, components of a cullin-RING ubiquitin ligase complex critical for thermotolerance and the intracellular pathogen response (IPR), including CUL-6 and SKR-5, were found to be specifically expressed in INT1 cells [49], suggesting that INT1 cells may play an integral role in proteostasis responses to intracellular pathogen infection. Collectively, these findings establish INT1 as a specialized cell-type that integrates endocrine, stress, and immune functions within the *C. elegans* intestine.

We uncovered pyruvate as a crucial metabolite that functions as a true surrogate for bacterial food to regulate the secretion of the endogenous insulin antagonist INS-7 [6]. Pyruvate must enter the TCA cycle to elicit this effect, suggesting that either actual metabolism of pyruvate is required, or that downstream metabolites may also act as mediators of this process. In other systems, TCA cycle intermediates such as acetyl-CoA, itaconate, and L-2-hydroxyglutarate (L-2-HG) modulate immune responses [50], while succinate and fumarate regulate hypoxia sensing upon cytosolic release [51]. A similar mechanism may underpin the communication between mitochondria and the nucleus in *C. elegans*, exemplified by the translocation of ATFS-1 during the activation of the mitochondrial unfolded protein response [52]. Thus, pyruvate metabolism may provide a metabolic checkpoint that couples nutrient availability to enteroendocrine signaling.

Many bacterial species including *Y. enterocolitica*, *C. freundii*, *E. aerogenes* and *E. coli* excrete pyruvate into the extracellular environment during nutrient-replete conditions [53, 54] and reabsorb extracellular pyruvate during nutrient insufficiency [55, 56]. Thus, the presence of extracellular pyruvate may serve as an indicator of the nutrient abundance in bacterial environments, a sensing mechanism that *C. elegans* may have co-evolved by leveraging the INT1 cells to couple environmental conditions with host physiology. It was reported that *C. elegans* exhibits chemotaxis to volatile pyruvic acid via AWC neurons [57]. However, the molecular mechanisms underlying both INT1 and neuronal sensing of pyruvate remain uncharacterized. Thus both intracellular and extracellular bacterial pyruvate appear to regulate the metabolism or behavior of *C. elegans*, indicating that pyruvate is a crucial signaling molecule.

In summary, we expect our TRAP-Seq datasets presented here to provide the scientific community with valuable resources for investigating the dynamic translatomes of specific subsets of intestinal cells in response to fasting and refeeding. More broadly, the discovery of cell-type heterogeneity within the *C. elegans* intestine highlights the evolutionary conservation of spatially organized intestinal biology and lays a foundation for future mechanistic studies of metabolic and immune regulation in the intestine.

Limitations of the TRAP-Seq in the current study

Not all previous studies have demonstrated a strong correlation between mRNA expression levels and protein abundance [58–60]. TRAP-Seq provides a more precise assessment of gene expression by detecting actively translating mRNAs. Specifically, TRAP-Seq better reflects the translational responses under various conditions, such as temperature fluctuations or fasting. Moreover, by employing tagged ribosomal proteins, TRAP-Seq enables the selective purification of polysomes without the need for cell dissociation or sorting, thereby reducing RNA contamination from neighboring cells or tissues.

To obtain sufficient ribosome-mRNA complexes for RNA sequencing, we generated strains with an integrated extrachromosomal array expressing HA-tagged RPL22 in either INT1 or INT2-9 cells. While this strategy enables robust affinity purification, the elevated expression of HA-tagged RPL22 in this system could potentially introduce unanticipated effects on transcript utilization or translational bias. Nevertheless, because all analyses rely on internal referencing, the differential gene expression signatures remain valid. In addition, the random integration of multi-copy transgenes into unknown genomic loci may alter the expression of adjacent genes, leading to additional variability. Importantly, we did not observe any changes in growth rate, fertility or fecundity in the TRAP-seq transgenic lines, suggesting that potential confounding effects are minimal.

TRAP has traditionally tagged proteins of the 60S large ribosomal subunit, including RPL10A [10, 11, 61–64] and RPL22 [13, 65–67], to enable tissue- or cell type-specific capture of polysome-mRNA complexes followed by RNA sequencing. A key distinction among previous studies lies in the choice of ribosomal protein for tagging. Both RPL10A and RPL22 are evolutionarily conserved ribosomal proteins. In *C. elegans*, RPL10A [64, 68, 69] and RPL22 [13, 67, 70] have been successfully used for tagging in TRAP-Seq experiments, yielding robust results. However, recent findings in mammalian systems indicate that RPL10A is significantly sub-stoichiometric in polysomes of mouse embryonic stem cells [71], suggesting it is not associated with all actively translating mRNAs. Similarly, in *C. elegans*, RPL10A shows limited expression in the germline and weak association with ribosomes, impairing the co-purification of translating mRNAs from the germline [70]. These observations suggest that tagging RPL10A in TRAP experiments may not capture the complete translatome in specific cell types or tissues. Further, *Nousch et al.* recently demonstrated that RPL-4 and RPL-9 are more effective than RPL10A and RPL22 for purifying polysome-mRNA complexes from germ cells in *C. elegans* [70], suggesting that the choice of ribosomal proteins for tagging in TRAP-Seq experiments may vary depending on the tissue of interest. Specifically, certain ribosomal proteins may offer improved specificity and efficiency for isolating tissue-specific mRNAs. Importantly, the RPL22-based TRAP in our experiments achieved robust immunoprecipitation efficiency (about 40% of input) for intestinal polysomal mRNAs (S4 table), thereby validating our approach. Future studies may further investigate whether alternative ribosomal proteins could provide enhanced isolation of translating mRNAs in different tissues including the intestine.

Materials and methods

C. elegans maintenance and strains

Worms were cultured on nematode growth medium (NGM) agar plates with *Escherichia coli* strain OP50 at 20°C as described [72]. Bristol strain N2 was obtained from the *Caenorhabditis* Genetic Center (CGC) and used as the wild-type strain. All transgenic strains used in this study are listed in

S1 Table. Worms were synchronized for Oil Red O staining by hypochlorite treatment, after which hatched L1 larvae were seeded on plates with the appropriate bacteria; worms were synchronized for INS-7 peptide secretion assay, PA14 avoidance and slow killing assays by letting gravid adult worms lay eggs on plates with the appropriate bacteria for 1.5 hr. All experiments were performed on day 1 adults.

Acute and chronic fasting

For the fasting experiments, synchronized day 1 adult worms were removed from the OP50 seeded NGM plates with M9 buffer, washed 3 times to remove remaining OP50 then placed on the unseeded NGM plates for 30 minutes (acute fast) or 180 minutes (chronic fast). For the refeeding experiments, fasted worms were removed from the fasting plate with M9 buffer then placed onto OP50 seeded plates for 30 minutes (acute fast/refeeding) or 90 minutes (chronic fast/refeeding).

Oil Red O staining

Oil Red O staining was performed as described [73]. Worms were harvested with phosphate-buffered saline (PBS) and incubated on ice for 10 minutes. Worms were fixed as described [73]. Following fixation, worms were stained in filtered Oil Red O (Thermo Scientific) working solution (60% Oil Red O in isopropanol: 70% water) overnight. Approximately 2000 worms were fixed and stained for all conditions within one experiment. We visually examined about 100 worms on slides and then blindly chose 20 worms for imaging. All experiments were repeated at least three times.

Image acquisition and quantitation

Oil Red O-stained worms were imaged using 10X objective on a Zeiss Axio Imager microscope. Images were acquired with the Software AxioVision (Zeiss). Lipid droplet staining in the first four pairs of intestinal cells was quantified using ImageJ software (NIH). All reported results were consistent across biological replicates. Fluorescent images of mNeonGreen reporters were acquired with software AxioVision (Zeiss) using a 10X objective on a Zeiss Axio Imager microscope. Fluorescent images of reporters for INS-7 secretion were acquired with software AxioVision (Zeiss) using a 20X objective on a Zeiss Axio Imager microscope. The images were taken at the indicated time point or immediately after treatment, such as refeeding. The first pair of coelomocytes was imaged. mCherry fluorescence intensity in one of the two imaged coelomocytes was quantified and normalized to the surface area of the coelomocyte (*Punc-122::GFP*) as previously described and validated [74]. Within each experiment, at least 15 worms from each condition were quantified using ImageJ software (NIH).

Cloning and transgenic strain construction

For generating *Pges-1ΔB::rpl-22-3xHA* and *Ppho-1::rpl-22-3xHA* constructs, promoters and *rpl-22-3xHA* were amplified with standard PCR techniques and subcloned into donor vectors using Gateway Cloning Technology™ (Life Technologies). All plasmids for NeonGreen reporters were generated by Gibson Assembly™. Primers used for cloning in this study are listed in S3 Table. Transgenic strains were generated by injecting plasmids into the germline of wild-type worms followed by visual selection of co-injection markers (*Pmyo-2::mCherry*, *Pges-1ΔB::GFP* or *Ppho-1::mCherry*) under the fluorescence microscope. The INS-7 secretion line was previously developed and validated [6]. For *INT1::TRAP* strain, N2 worms were injected with 10 ng/μL of the *Pges-1ΔB::rpl-22-3xHA* plasmid, 20 ng/μL of the *Pges-1ΔB::GFP* plasmid, and 70 ng/μL of an empty vector to bring the final concentration of injection mix to 100 ng/μL. For *INT2-9::TRAP* strain, N2 worms were injected with 25 ng/μL of the *Ppho-1::rpl-22-3xHA* plasmid, 50 ng/μL of the *Ppho-1::mCherry* plasmid, and 25 ng/μL of an empty vector to bring the final concentration of injection mix to 100 ng/μL. A transgenic line with high transmission rate and consistent expression was integrated using the Stratalinker UV Crosslinker 2400 (Stratagene) and backcrossed four times before experimentation. For other microinjections, we injected the animals with 30 ng/μL of the desired

plasmid, 10 ng/µL of the *Pmyo-2::mCherry* and 60 ng/µL empty vector to maintain a final injection mix concentration of 100 ng/µL. Two lines were selected for experimentation based on the transmission rate and consistency of expression.

RNAi

RNAi experiments were performed as described [75, 76]. Carbenicillin-IPTG plates were seeded with HT115 bacteria containing the empty or the relevant RNAi clone four days before seeding larvae.

PA14 avoidance assay

The PA14 avoidance assay was performed as previously described [77]. *Pseudomonas aeruginosa* strain PA14 was cultured by inoculating a single colony into 2 mL of LB broth and incubating at 37 °C for 6 hr. 20 µL of the culture was then seeded onto 3.5 cm slow-killing (SK) plates and incubated at 37 °C for 15 hr. For each assay, 30 synchronized Day 1 gravid adults (containing 6-10 eggs) grown on RNAi bacteria were cleaned and transferred to the agar surface outside the PA14 lawn. The number of animals on and off the PA14 lawns was scored after 8 h. Three plates were used per RNAi treatment in each experiment.

PA14 slow killing assay

PA14 slow killing assay was performed as described [30]. Briefly, overnight cultures of *Pseudomonas aeruginosa* strain PA14 were seeded onto slow-killing (SK) plates and incubated at 37°C for 24 hr, followed by 25°C for an additional 24 hr. Synchronized animals at the closed vulva stage subjected to RNAi treatment were transferred to 3.5 cm SK plates seeded with PA14 (30 animals per plate), with three plates per RNAi treatment. Plates were maintained at 25°C, and worm survival was monitored until all animals had died. Survival curves were analyzed using GraphPad Prism, and statistical significance was determined by the log-rank test.

Translating ribosome affinity purification

The protocol was adapted from reference [13] and described in detail in S1 Protocol. Briefly, transgenic worms containing the Ribo-TRAP constructs were made to drive expression of *rpl-22-3xHA* in INT1 and INT2-9. Age-matched transgenic worms for each experimental condition were washed, flash-frozen, and lysed to release ribosomes and cellular components in the presence of cycloheximide to pause translation as well as RNAase and protease inhibitors. Immunoprecipitation of ribosomes from our desired tissue was performed with a monoclonal anti-HA antibody and protein G-beads. Nascent RNA was eluted from ribosomes with beta mercaptoethanol (BMP). Percent IP RNA compared to input, on average less then 1%, was used to determine if the IP was successful.

RNA purification

RNA from the IP, flowthrough, and input was purified with Agilent Absolutely RNA Nanoprep Kit^{TM} according to the manufacturer's instructions including the on-column DNase treatment. Final RNA isolates were eluted in 15 µl and used to make diluted aliquots for sequencing, validation, and QC.

RNA quality assessment

We tested for RNA degradation and quality by running the input, flowthrough, and IP samples on an Agilent Bioanalyzer chip (nano or pico, depending on concentration). Because IP samples had a small concentration it was difficult to accurately measure the RNA integrity number (RIN) in all conditions, but the quality of RNA for these unknown samples could be extrapolated from the flowthrough and input samples. In all conditions the average RIN across sample types was greater than 7.5 indicating a RNA integrity sufficient for sequencing, and in the majority of conditions it was greater than 9 indicative of high-quality samples.

RNAseq library prep, sequencing, and alignment

Total RNA samples were prepared into RNAseq libraries using the NEBNext® Ultra™ Directional RNA Library Prep Kit for Illumina® following the manufacturer's recommended protocol. Briefly, for each sample 100ng total RNA was polyA-selected, converted to double stranded cDNA followed by fragmentation and ligation of sequencing adapters. The libraries were then PCR amplified 12 cycles using barcoded PCR primers, purified and size selected using AMPure XP Beads before loading onto an Illumina NextSeq500 for 75 base single read sequencing. Reads were aligned to *C. elegans* genome (WBcel235/r67) using STAR (version 2.6.1d) [78], and gene counts were produced using featureCounts (version 1.6.4) [79]. On average, 10.6 million unique single-end (SE) reads aligned per INT1 sample and 19.5 million unique SE reads per INT2-9 sample, differences were due to the larger RNA input for INT2-9 samples. Data quality was assessed using FastQC (version 0.11.8) [80]. Raw RNA-seq FASTQ files and a gene count matrix are available on GEO (GSE306302). Bioinformatic analysis was performed using R programming language (version 4.4.2) (R Development Core Team, 2015) and RStudio integrated development environment (version 2024.12.1) (Team R, 2018). Plots were generated using ggplot2 R package (version 3.5.2).

Differential expression analysis

Differential expression analysis was performed using the DESeq2 R package (version 1.46.0) [81] which models the gene expression counts with a negative binomial distribution while adjusting for library size and dispersion. Differentially expressed genes were identified as having adjusted p-value less then 0.05 using a Benjamini-Hochberg false discovery rate correction. DESeq2 variance stabilized counts were used to generate normalized count matrices that were used for plotting expression data of individual genes and those averaged across WGCNA modules. PCA was performed using the top 500 variable genes from variance stabilized counts output in DESeq2. Statistical significance of PCA correlation was determined with a Pearson's correlation for 2 factor comparisons (line) or an ANOVA for multi-factor comparisons (metabolic stress). Plot ellipses comparing groups were drawn with ggplot2 stat_ellipse() function which computes the mean and covariance of the PC1 and PC2 for each line to build the ellipse at a 95% confidence level.

WGCNA

WGCNA was performed with the WGCNA R package (version 1.73) [16] to identify modules of co-expressed genes and their associations with external traits in the analysis. Prior to analysis, samples with low expression values were removed to reduce variation associated with batch, a 30 min fasting and 30 min refeeding sample were removed from the *Pges-1ΔB* experiment based on this criteria. DESeq2 variance stabilized counts were used as the input and only genes in the 95th percentile of variance were kept to reduce noise (n = 2,338). A soft-thresholding power of 10 was selected using the scale-free topology criterion to approximate scale-free network topology. A signed adjacency matrix was constructed and transformed into a topological overlap matrix (TOM), followed by hierarchical clustering to detect modules of highly correlated genes. Modules were identified using dynamic tree cutting with a minimum module size of 30 genes and subsequently merged based on eigengene similarity (cut height = 0.25). Module eigengenes (MEs) were correlated with external traits (e.g., line and fasting condition), and Pearson correlation coefficients along with associated p-values were computed. Modules showing significant trait associations were further investigated for biological relevance and functional enrichment. Module GO enrichment analysis was performed using the ClusterProfiler R package version (version 4.14.6)[82]. For GO analysis, we reported terms with FDR < 0.1. The test set of module genes was compared against the background set of genes in the WGNCA analysis passing the variance criteria.

Statistics

Wild-type animals were included as controls for every experiment. Error bars represent standard error of the mean (SEM). Student's *t*-test and one-way ANOVA were used as indicated in the Fig legends. All statistical analyses were performed in GraphPad Prism 9.3 (GraphPad Software).

Appropriate multiple comparison corrections were used for ANOVAs.

Supplementary figures

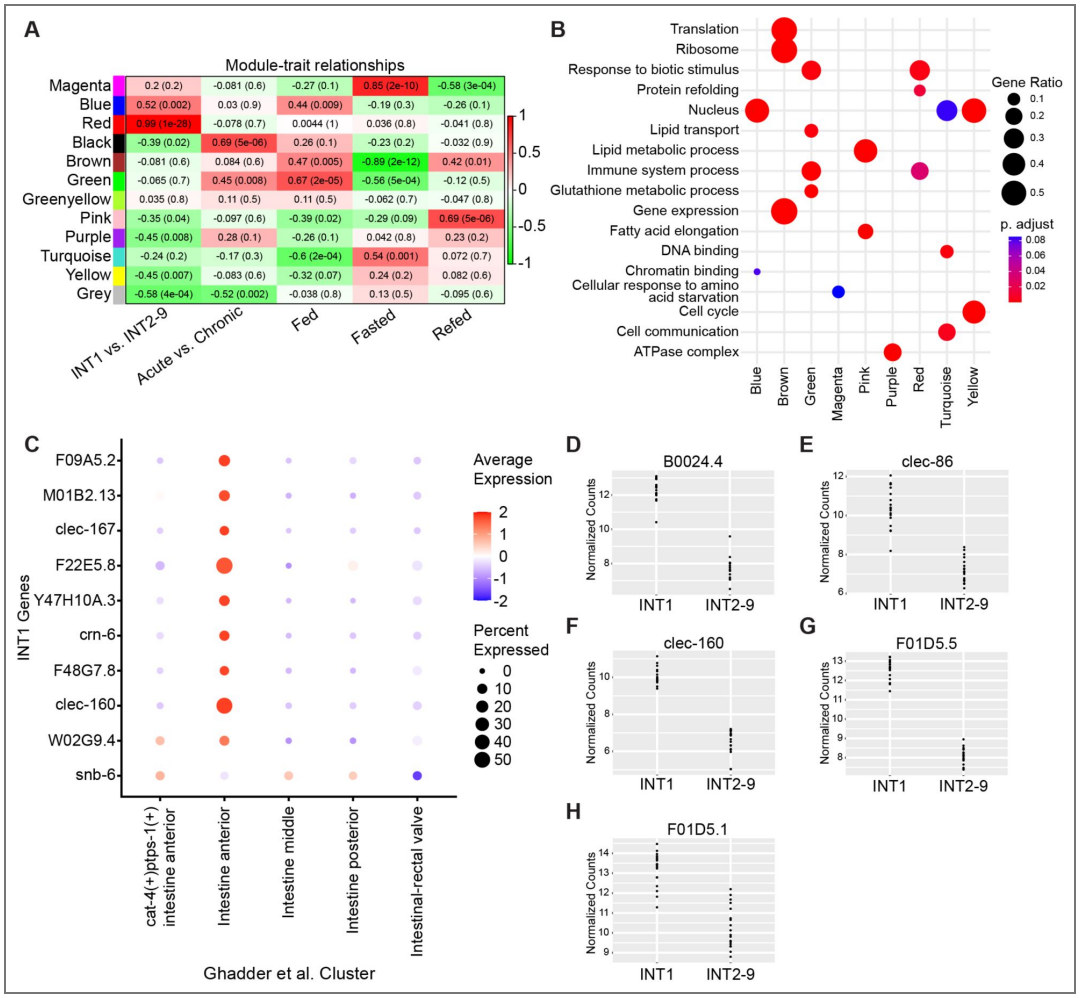

S1 Fig. The genes differentially expressed in INT1 cells. (A) Module-trait relationships for selected conditions in WGCNA. Rows indicate the WGCNA module and the columns comparative traits. The color indicates the strength of the Pearson's correlation and bracketed number the significance. The color red represents a positive correlation; the color green represents a negative correlation. (B) GO enrichment of selected modules in the WGCNA analysis. Size indicates the strength of the significance and color the significance. (C) Dotplot showing increased expression in the anterior intestine clusters from Ghadder et al. for genes upregulated in the INT1 vs INT2-9 Fed datasets. We selected the top 10 significant (FDR < 0.05) genes ranked by effect size that were expressed in at least 5% of anterior intestinal cells to show. Size indicates the percent of cells expressing the gene, and color indicates the scaled effect size. (D-H) Expression profiles of *B0024.4, clec-86, clec-160, F01D5.5* and *F01D5.1* under all conditions in INT1 and INT2-9 cells.

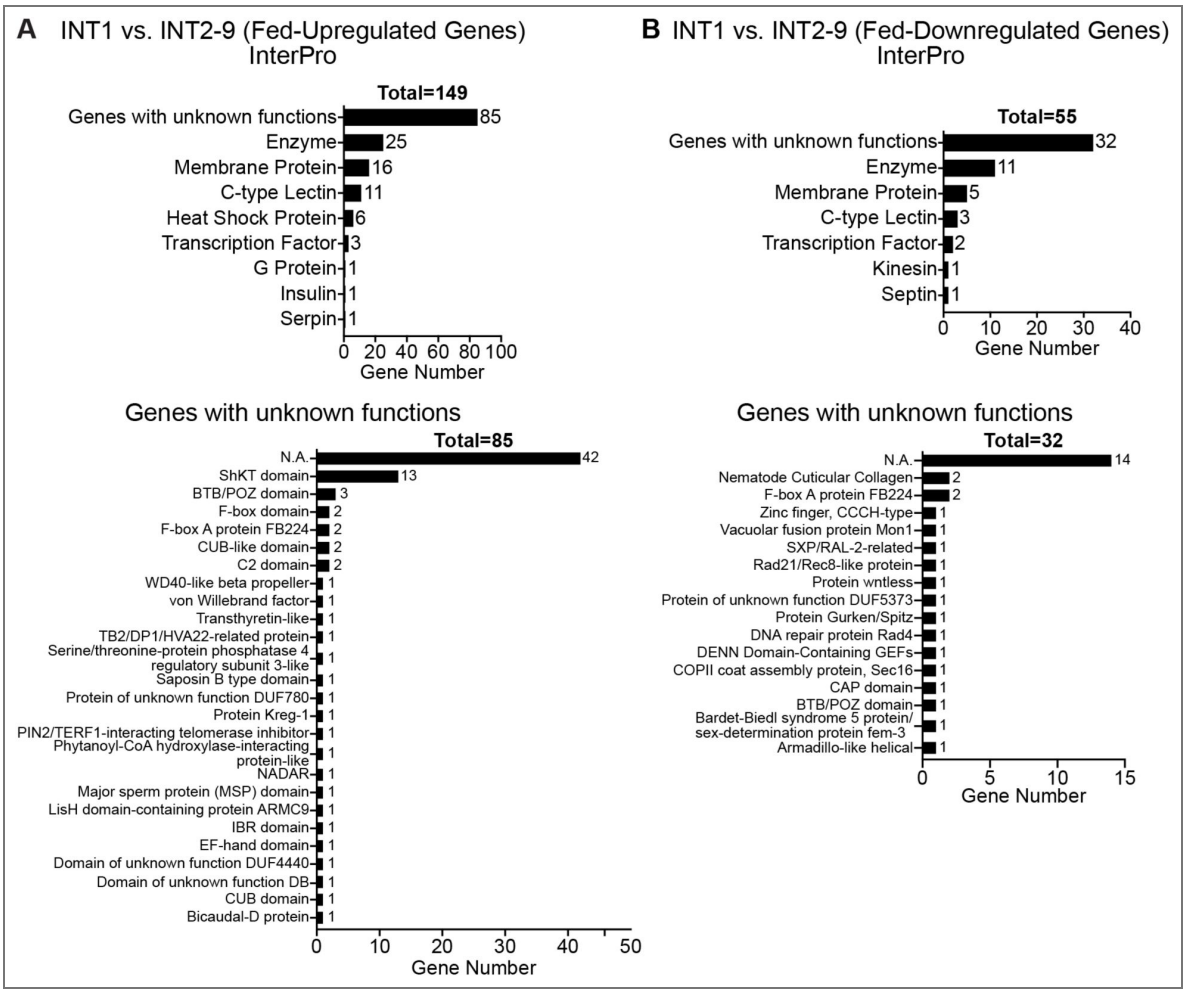

S2 Fig. InterPro annotations of differentially expressed genes for INT1 Fed versus INT2-9 Fed.

(A, B) Bar charts of the upregulated or downregulated genes categorized by the protein domains predicted by InterPro for INT1 fed versus INT2-9 fed.

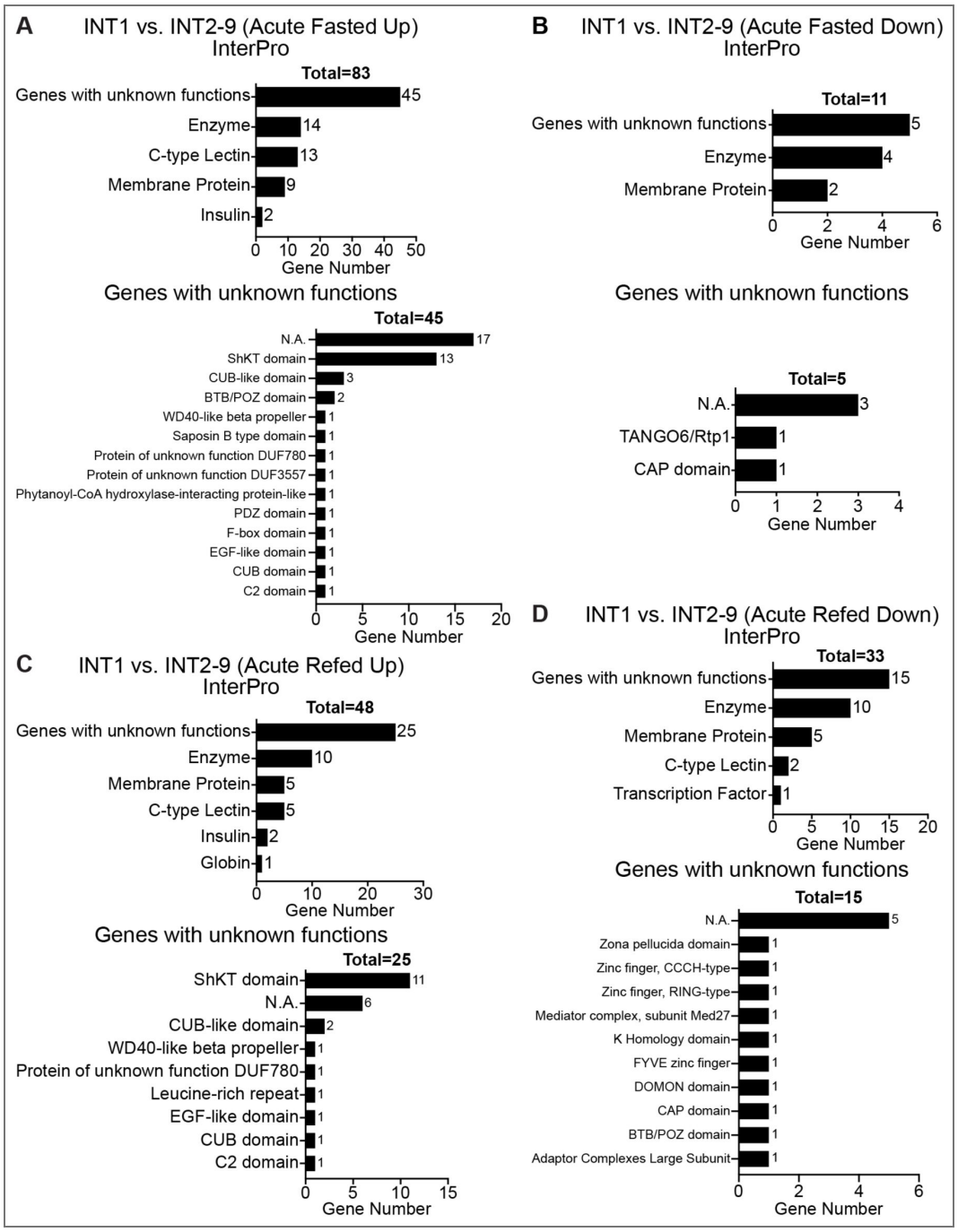

S3 Fig. InterPro annotations of differentially expressed genes for INT1 versus INT2-9 under acute conditions.

(A, B) Bar charts of the upregulated or downregulated genes categorized by the protein domains predicted by InterPro for INT1 30 min fasted versus INT2-9 30 min fasted. (C, D) Bar charts of the upregulated or downregulated genes categorized by the protein domains predicted by InterPro for INT1 30 min refed versus INT2-9 30 min refed.

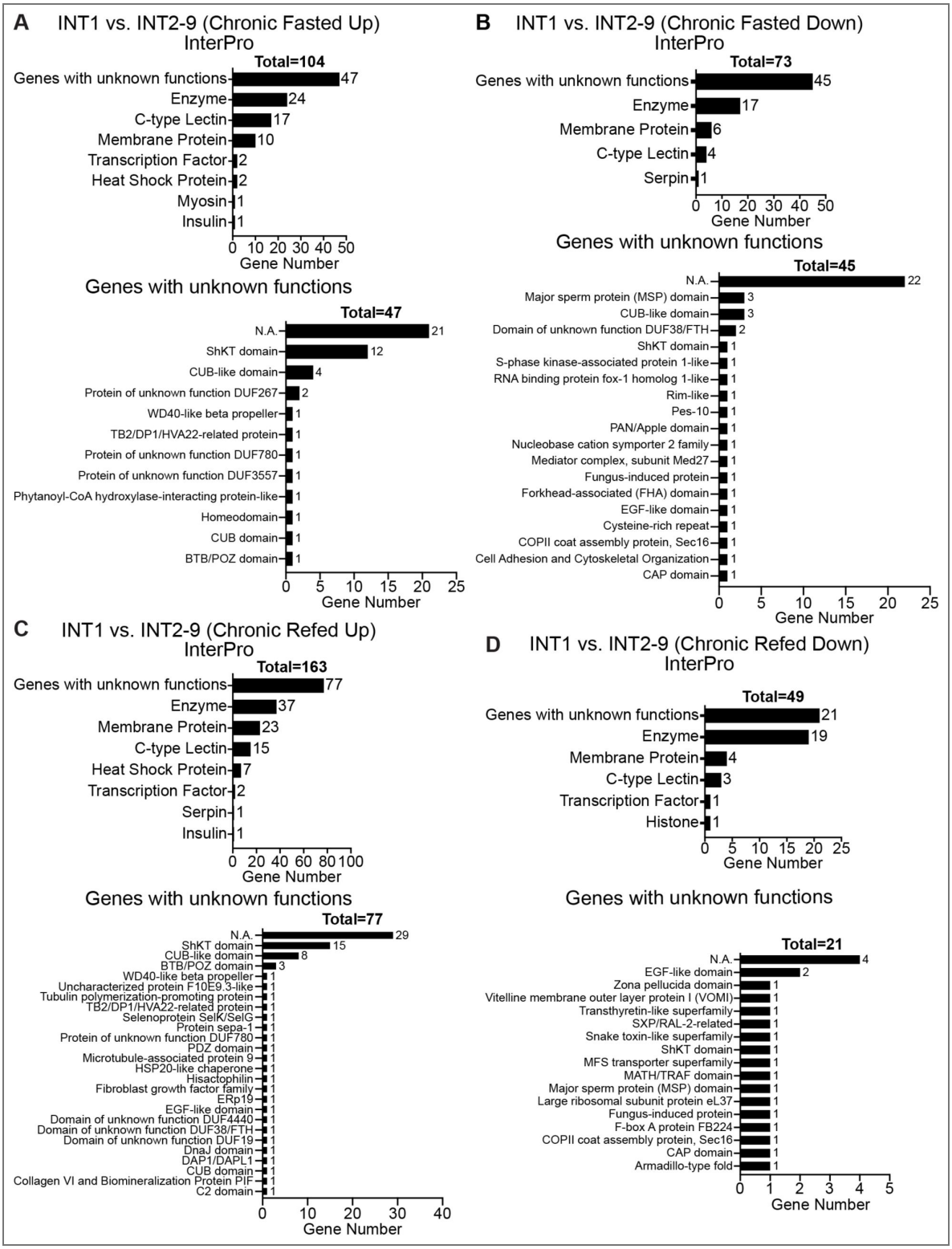

S4 Fig. InterPro annotations of differentially expressed genes for INT1 versus INT2-9 under chronic conditions.

(A, B) Bar charts of the upregulated or downregulated genes categorized by the protein domains predicted by InterPro for INT1 180 min fasted versus INT2-9 180 min fasted. (C, D) Bar charts of the upregulated or downregulated genes categorized by the protein domains predicted by InterPro for INT1 90 min refed versus INT2-9 90 min refed.

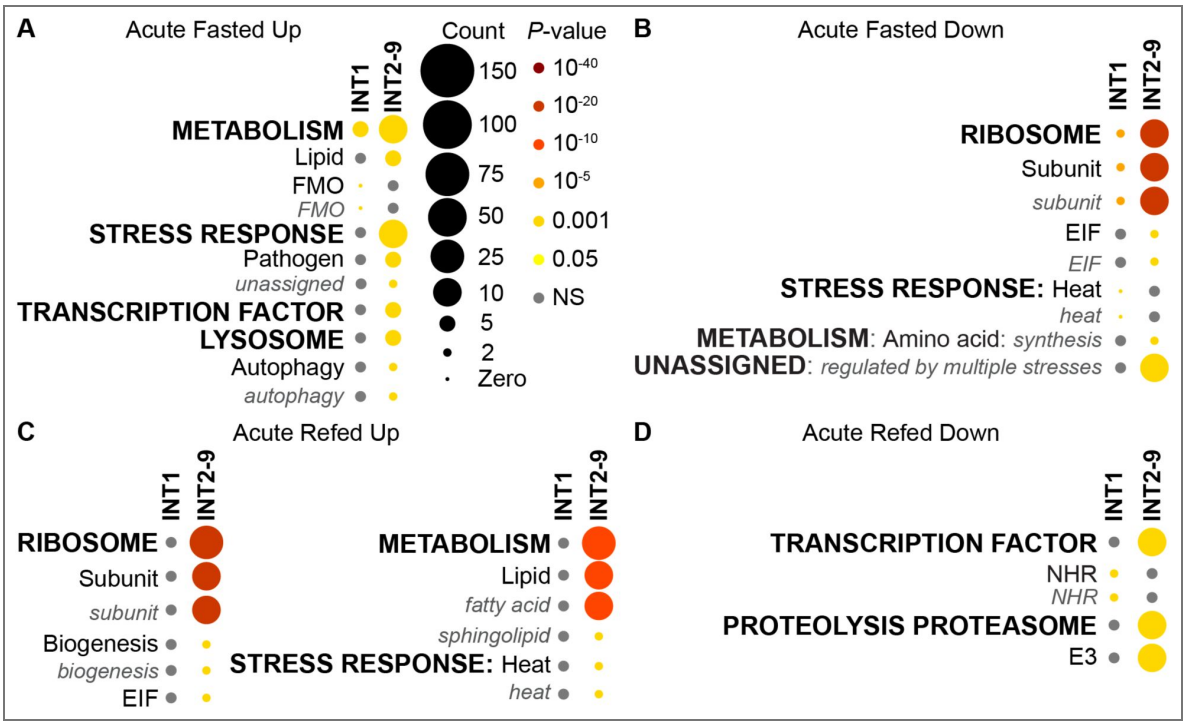

S5 Fig. WormCat annotations of differentially expressed genes under acute fasting and refeeding conditions for INT1 and INT2-9 cells.

(A, B) WormCat visualization of categories enriched in differentially expressed genes in INT1 cells and INT2-9 cells under acute fasting condition. (C, D) WormCat visualization of categories enriched in differentially expressed genes in INT1 cells and INT2-9 cells under acute refeeding condition. Categories 1 are all bold uppercase; Categories 2 are capitalized; Categories 3 are gray italics. The size of the bubbles indicates the gene counts in the category and the color of the bubble represents the adjusted p-value.

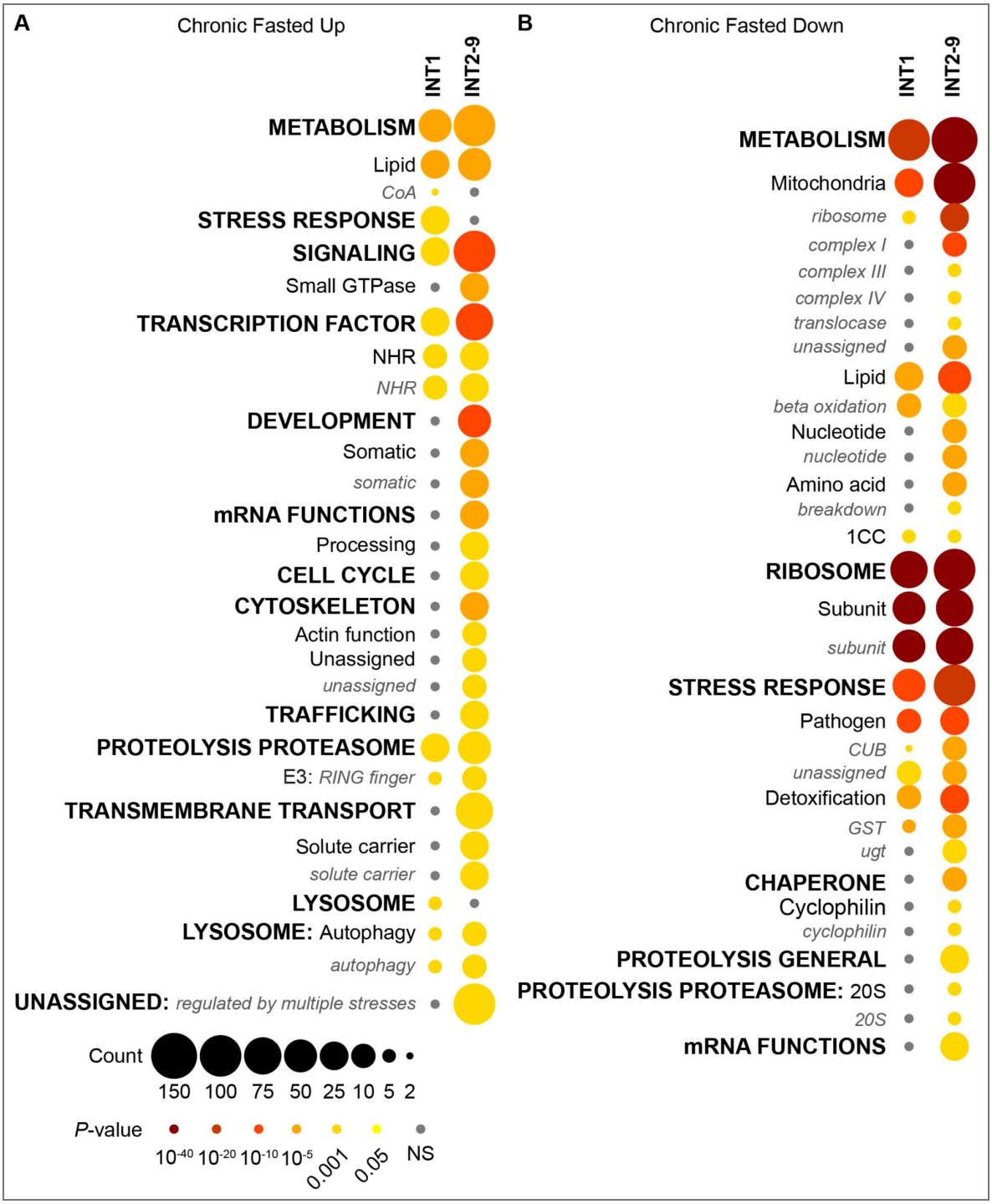

S6 Fig. WormCat annotations of differentially expressed genes under chronic fasting condition for INT1 and INT2-9 cells.

(A, B) WormCat visualization of categories enriched in differentially expressed genes in INT1 cells and INT2-9 cells under chronic fasting condition. Categories 1 are all bold uppercase; Categories 2 are capitalized; Categories 3 are gray italics. The size of the bubbles indicates the gene counts in the category and the color of the bubble represents the adjusted p-value.

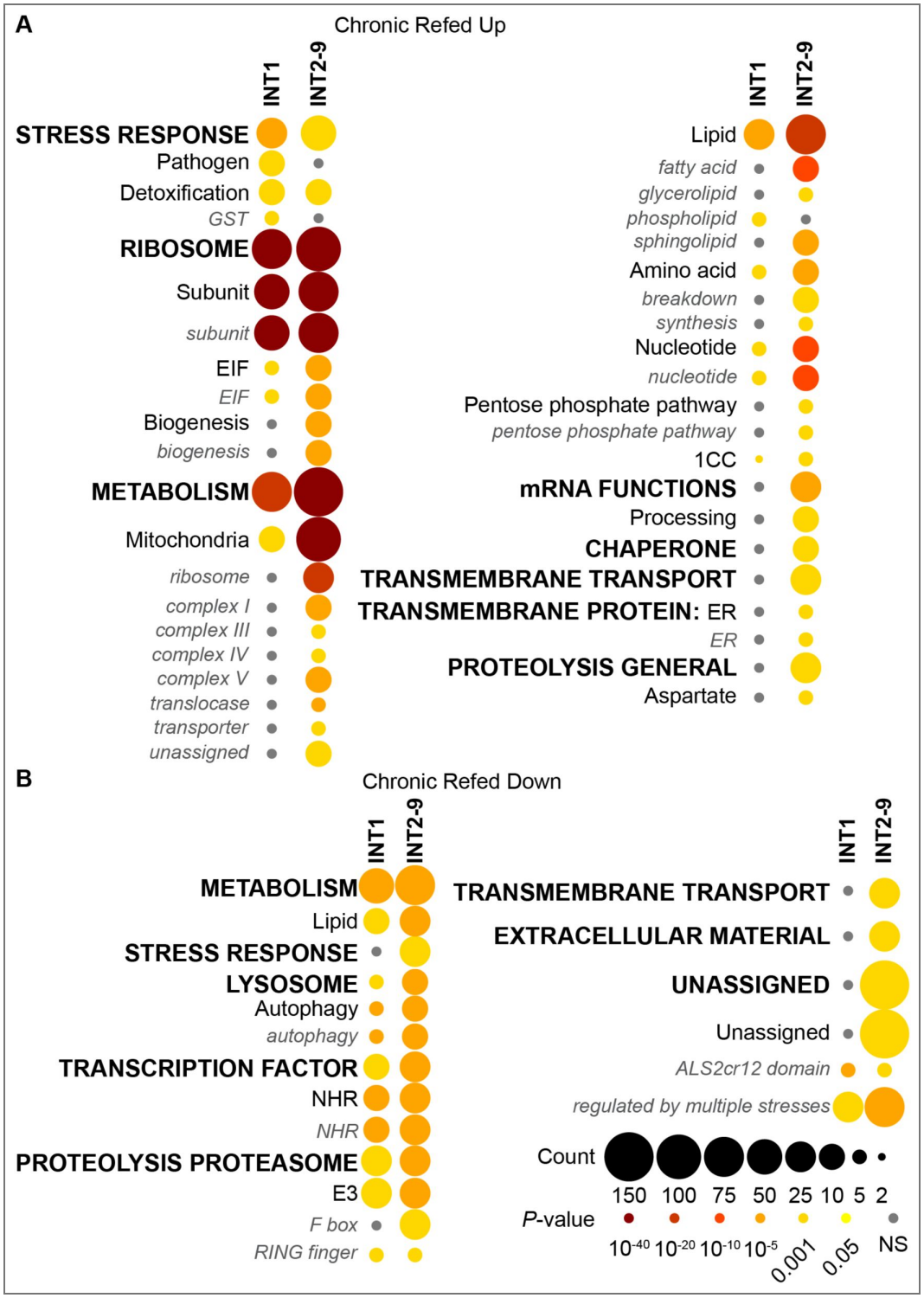

S7 Fig. WormCat annotations of differentially expressed genes under chronic refeeding condition for INT1 and INT2-9 cells.

(A, B) WormCat visualization of categories enriched in differentially expressed genes in INT1 cells and INT2-9 cells under chronic refeeding condition. Categories 1 are all bold uppercase; Categories 2 are capitalized; Categories 3 are gray italics. The size of the bubbles indicates the gene counts in the category and the color of the bubble represents the adjusted p-value.

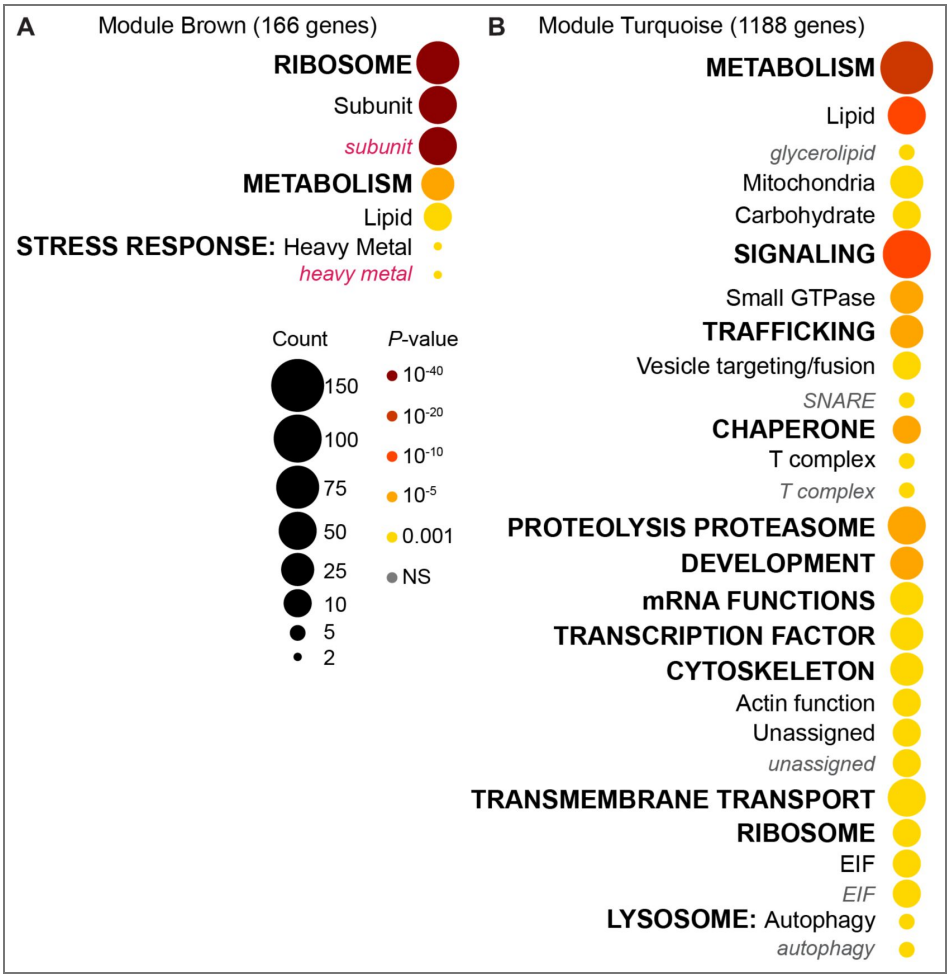

S8 Fig. WormCat annotations of undulating genes in INT1 and INT2-9 cells.

(A, B) WormCat visualization of categories enriched in genes of module brown and turquoise. Categories 1 are all bold uppercase; Categories 2 are capitalized; Categories 3 are gray italics. The size of the bubbles indicates the gene counts in the category and the color of the bubble represents the adjusted p-value.

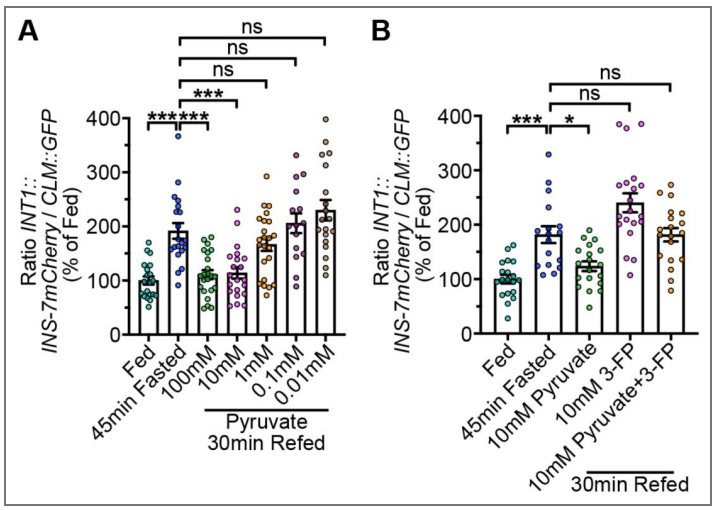

S9 Fig. The role of pyruvate in refeeding responses of INS-7 secretion from INT1 cells.

(A) INS-7 secretion dynamics during fasting and re-feeding with different concentrations of pyruvate (0.01 mM - 100 mM) were determined at the indicated time points. The intensity of INS-7mCherry fluorescence within a single coelomocyte was quantified and normalized to the area of CLM::GFP expression for each time point. Data are expressed as a percentage of the normalized INS-7mCherry fluorescence intensity of wild-type fed animals ± SEM (n=15-23). ***p<0.001, ^{ns}p>0.05 by one-way ANOVA (Dunnett T3). (B) INS-7 secretion dynamics during fasting and re-feeding with 10 mM pyruvate, 10 mM 3-FP, and 10 mM pyruvate and 3-FP were determined at the indicated time points. The intensity of INS-7mCherry fluorescence within a single coelomocyte was quantified and normalized to the area of CLM::GFP expression for each time point. Data are expressed as a percentage of the normalized INS-7mCherry fluorescence intensity of wild-type fed animals ± SEM (n=17-20). *p<0.05, ***p<0.001, ^{ns}p>0.05 by one-way ANOVA (Dunnett T3).

Supplementary tables

Strains used in this study	Source	Identifier	Additional Information
N2; ssrIs1248[Pges-1ΔB::rpl-22-3xHA]; ssrIs1191[Pges-1ΔB::GFP]	This paper	SSR1578	Integrated. Backcrossed 4X.
N2; ssrIs1191[Pges-1ΔB::GFP]; ssrIs1210[Ppho-1::mCherry]	This paper	SSR1582	Integrated. Backcrossed 4X.
N2; ssrIs1251[Ppho-1::rpl-22-3xHA]; ssrIs1210[Ppho-1::mCherry]	This paper	SSR1605	Integrated. Backcrossed 4X.
sid-1(qt9); ssrIs1220[Pges-1ΔB::sid-1::GFP]; ssrIs1240[Pges-1ΔB::ins-7mCherry]; ssrIs615[Punc-122::GFP]	PMID: 37961386	SSR1634	
N2; ssrEx1317[Pclec-160::mNeonGreen]; ssrEx1031[Pmyo-2::mCherry]	This paper	SSR1701	
N2; ssrEx1319[Pclec-86::mNeonGreen]; ssrEx1031[Pmyo-2::mCherry]	This paper	SSR1702	
N2; ssrEx1318[PB0024.4::mNeonGreen]; ssrEx1031[Pmyo-2::mCherry]	This paper	SSR1703	
N2; ssrEx1323[PF01D5.5::mNeonGreen]; ssrEx1031[Pmyo-2::mCherry]	This paper	SSR1705	
N2; ssrEx1324[Pnpr-28::mNeonGreen]; ssrEx1031[Pmyo-2::mCherry]	This paper	SSR1706	
N2; ssrEx1325[PF01D5.1::mNeonGreen]; ssrEx1031[Pmyo-2::mCherry]	This paper	SSR1713	

Supplementary Table 1. ***C. elegans*** **strains used in this study.**

Plasmids used in this study	Source	Identifier
Pges-1ΔB::GFP	This paper	pSS1191
Ppho-1::mCherry	This paper	pSS1210
Pges-1ΔB::rpl-22-3xHA	This paper	pSS1248
Ppho-1::rpl-22-3xHA	This paper	pSS1251
Pclec-160::mNG::clec-160 3'UTR	This paper	pSS1317
PB0024.4::mNG::B0024.4 3'UTR	This paper	pSS1318
Pclec-86::mNG::clec-86 3'UTR	This paper	pSS1319
PF01D5.5::mNG::F01D5.5 3'UTR	This paper	pSS1323
Pnpr-28::mNG::npr-28 3'UTR	This paper	pSS1324
PF01D5.1::mNG::F01D5.1 3'UTR	This paper	pSS1325

Supplementary Table 2. Plasmids used in this study.

Gibson Assembly	Primer	Source	Sequence
Pclec-160::mNG::clec-160 3'UTR	Forward primer for cloning the *Pclec-160* sequence	IDT	CATGCCTGCAAGGAAAAAATTGGAAGGGAAAGGAAAACT
	Reverse primer for cloning the *Pclec-160* sequence	IDT	TTGGAGACCATCTGAATAATTCTTGGGTATTAAAAAAAAGATTTTTGTACCTATTGG
	Forward primer for cloning the mNG sequence	IDT	AATTATTCAGATGGTCTCCAAGGGAGAGGAG
	Reverse primer for cloning the mNG sequence	IDT	GAATGACATCACTACTTGTAGAGCTCGTCCATTCC
	Forward primer for cloning the *clec-160 3'UTR* sequence	IDT	CTACAAGTAGTGATGTCATTCTCAATTTGAATTTAAACAGAATAAACTATTTTTAAAAGT
	Reverse primer for cloning the *clec-160 3'UTR* sequence	IDT	AATTCGAGCTCTCGCCTCAATTCTGTGATTCATAAAAAGTTCA
	Forward primer for cloning the pUC19 sequence	IDT	ATTGAGGCGAGAGCTCGAATTCACTGGCCG
	Reverse primer for cloning the pUC19 sequence	IDT	AATTTTTTCCTTGCAGGCATGCAAGCTTG
Pclec-86::mNG::clec-86 3'UTR	Forward primer for cloning the *Pclec-86* sequence	IDT	AGCTTGCATGCCTACCCGACCGGCCG
	Reverse primer for cloning the *Pclec-86* sequence	IDT	CCTTGGAGACCATTTTCAGTGTCCAGTAAAATAATAAATTTTATCTGCTTATCACAG
	Forward primer for cloning the mNG sequence	IDT	CTGGACACTGAAAATGGTCTCCAAGGGAGAGGAG
	Reverse primer for cloning the mNG sequence	IDT	TTCGAATCAAAAGCTACTTGTAGAGCTCGTCCATTCCC
	Forward primer for cloning the *clec-86 3'UTR* sequence	IDT	GCTCTACAAGTAGCTTTTGATTCGAAAGAAAATATTTATATATTATGAGCTAAATTGGAT
	Reverse primer for cloning the *clec-86 3'UTR* sequence	IDT	GTGAATTCGAGCTACCTGAGCATGCCGTTTGG

Supplementary Table 3. Cloning primers used in this study.

	Forward primer for cloning the pUC19 sequence	IDT	GGCATGCTCAGGTAGCTCGAATTC ACTGGCCGTCGTTTTACA
	Reverse primer for cloning the pUC19 sequence	IDT	CGGCCGGTCGGGTAGGCATGCAA GCTTGGCGT
PB0024.4::mNG::B0024.4 3'UTR	Forward primer for cloning the *PB0024.4* sequence	IDT	CTTGCATGCCTGTTTAATTTTAAATG AGAAAATAATGATTTTTTGTCATTAA ATTTAACT
	Reverse primer for cloning the *PB0024.4* sequence	IDT	CTTGGAGACCATTCTACTAGAAATA GAAAGTTCGTTTGGAATACCG
	Forward primer for cloning the mNG sequence	IDT	TTTCTAGTAGAATGGTCTCCAAGGG AGAGGAG
	Reverse primer for cloning the mNG sequence	IDT	ACAAATATCAACCTACTTGTAGAGC TCGTCCATTCCC
	Forward primer for cloning the *B0024.4 3'UTR* sequence	IDT	TCTACAAGTAGGTTGATATTTGTTTG TAATTACGGACTTATGGTGC
	Reverse primer for cloning the *B0024.4 3'UTR* sequence	IDT	AGTGAATTCGAGATTATTTGTGGCC ATCCCCAACTATAAAAAT
	Forward primer for cloning the pUC19 sequence	IDT	CCACAAATAATCTCGAATTCACTGG CCGTCG
	Reverse primer for cloning the pUC19 sequence	IDT	TTAAAATTAAACAGGCATGCAAGCT TGGCGT
PF01D5.5::mNG::F01D5.5 3'UTR	Forward primer for cloning the *PF01D5.5* sequence	IDT	AGCTTGCATGCCCTGGAAATTGTTC GGGGATTTTTAATTTTTTTTTAAGC
	Reverse primer for cloning the *PF01D5.5* sequence	IDT	CCTTGGAGACCATCGCGAGCTTGA AGTTTTTCTTTGTT
	Forward primer for cloning the mNG sequence	IDT	TTCAAGCTCGCGATGGTCTCCAAG GGAGAGGAG
	Reverse primer for cloning the mNG sequence	IDT	ATTTTTGTAATTACTACTTGTAGAGC TCGTCCATTCC
	Forward primer for cloning the *F01D5.5 3'UTR* sequence	IDT	CTCTACAAGTAGTAATTACAAAAATA TCTTTGGAATTGTAAATATTGTTATTT GAATAAA
	Reverse primer for cloning the *F01D5.5 3'UTR* sequence	IDT	ATTCGAGCTCGGTTGCCGTTCCCC TATCCTACCGTAC
	Forward primer for cloning the pUC19 sequence	IDT	AGGGGAACGGCAACCGAGCTCGA ATTCACTGGCC
	Reverse primer for cloning the pUC19 sequence	IDT	GAACAATTTCCAGGGCATGCAAGC TTGGCGT
PF01D5.1::mNG::F01D5.1 3'UTR	Forward primer for cloning the *PF01D5.1* sequence	IDT	CAAGCTTGCATGCCTGGATAAAGAA AGCATGAATTTGAATTTTATATGTAC ACTATTCT
	Reverse primer for cloning the *PF01D5.1* sequence	IDT	TCCCTTGGAGACCATTTGTTTTCTG CAAAACTTAGTTTTTAGATAAAATGA CTTTAAGAC
	Forward primer for cloning the mNG sequence	IDT	TTTGCAGAAAACAAATGGTCTCCAA GGGAGAGGAG
	Reverse primer for cloning the mNG sequence	IDT	AATAAAAAGATTTATCTACTTGTAGA GCTCGTCCATTCCC
	Forward primer for cloning the *F01D5.1 3'UTR* sequence	IDT	AGCTCTACAAGTAGATAAATCTTTTT ATTTTAATTTTCATCGTAACTCGGTA GTAGAACA
	Reverse primer for cloning the *F01D5.1 3'UTR* sequence	IDT	CAGTGAATTCGAGCTCAGACACAC TACACCTAACTCGTTCAG
	Forward primer for cloning the pUC19 sequence	IDT	GTGTAGTGTGTCTGAGCTCGAATTC ACTGGCCG
	Reverse primer for cloning the pUC19 sequence	IDT	TGCTTTCTTTATCCAGGCATGCAAG CTTGGCGT
Pnpr-28::mNG::npr-28 3'UTR	Forward primer for cloning the *Pnpr-28* sequence	IDT	TTGCATGCCTGAGCTAATGTCCTAT TCGCCCC
	Reverse primer for cloning the *Pnpr-28* sequence	IDT	TTGGAGACCATAGTAGAATAACTGA CAAGTCGTGTAAAGCAAA
	Forward primer for cloning the mNG sequence	IDT	GTTATTCTACTATGGTCTCCAAGGG AGAGGAG
	Reverse primer for cloning the mNG sequence	IDT	AGTATTGTTATCTACTTGTAGAGCTC GTCCATTCCC
	Forward primer for cloning the *npr-28 3'UTR* sequence	IDT	TCTACAAGTAGATAACAATACTTTGA ATATGTACCTTTTTTCAACTTGTATC ATT

Supplementary Table 3. (continued)

	Reverse primer for cloning the *npr-28 3'UTR* sequence	IDT	TGAATTCGAGCTATTTCGTAATATTT ATTTGTTTATCTTTTTATTTACTTATTT CACTCA
	Forward primer for cloning the pUC19 sequence	IDT	ATTACGAAATAGCTCGAATTCACTG GCCG
	Reverse primer for cloning the pUC19 sequence	IDT	GGACATTAGCTCAGGCATGCAAGC TTGGCGT

Supplementary Table 3. (continued)

Data availability

RNA sequence data were deposited in GEO (accession number GSE306302). All data generated or analyzed during this study are included in the manuscript and supporting files; source data files have been provided for all figures.

Acknowledgements

This work was supported by research grants to S.S. from the NIH/NIDDK (R01 DK124706) and NIH/NIA (R01 AG056648). This work was supported by the resources and staff at the Scripps Research Genomics Core Facility. C.L. was supported by a Dorris Scholar Award from the Dorris Neuroscience Center, The Scripps Research Institute.

Additional files

Supplemental Table 4

Supplemental Table 5

Supplemental Table 6

Supplemental Table 7

Source Data 1

Additional information

Funding

Funder	Grant reference number	Author
HHS | National Institutes of Health (NIH)	R01 DK124706	Supriya Srinivasan
HHS | National Institutes of Health (NIH)	R01 AG056648	Supriya Srinivasan

Author ORCID iDs

Chung-Chih Liu: https://orcid.org/0000-0001-6164-4393
Supriya Srinivasan: https://orcid.org/0000-0003-2544-3652

References

1. **Ghafouri S,** McGhee JD (2007) Bacterial residence time in the intestine of Caenorhabditis elegans. *Nematology* **9**:87-91 https://doi.org/10.1163/156854107779969718
2. **Van Gilst MR,** Hadjivassiliou H, Yamamoto KR (2005) A Caenorhabditis elegans nutrient response system partially dependent on nuclear receptor NHR-49. *Proc Natl Acad Sci U S A* **102**:13496-501 https://doi.org/10.1073/pnas.0506234102 | PubMed
3. **O'Rourke EJ,** Ruvkun G (2013) MXL-3 and HLH-30 transcriptionally link lipolysis and autophagy to nutrient availability. *Nat Cell Biol* **15**:668-76 https://doi.org/10.1038/ncb2741 | PubMed
4. **Jo H,** Shim J, Lee JH, Lee J, Kim JB (2009) IRE-1 and HSP-4 contribute to energy homeostasis via fasting-induced lipases in C. elegans. *Cell Metab* **9**:440-8 https://doi.org/10.1016/j.cmet.2009.04.004 | PubMed
5. **Sulston JE,** Schierenberg E, White JG, Thomson JN (1983) The embryonic cell lineage of the nematode Caenorhabditis elegans. *Dev Biol* **100**:64-119 https://doi.org/10.1016/0012-1606(83)90201-4 | PubMed
6. **Liu CC,** Khan A, Seban N, Littlejohn N, Shah A, Srinivasan S (2024) A homeostatic gut-to-brain insulin antagonist restrains neuronally stimulated fat loss. *Nat Commun* **15**:6869 https://doi.org/10.1038/s41467-024-51077-3 | PubMed

7. **Quintin S,** Aspert T, Ye T, Charvin G (2022) Distinct mechanisms underlie H2O2 sensing in C. elegans head and tail. *PLoS One* **17**:e0274226 https://doi.org/10.1371/journal.pone.0274226 | PubMed
8. **Warner JR,** Knopf PM (2002) The discovery of polyribosomes. *Trends Biochem Sci* **27**:376-80 https://doi.org/10.1016/s0968-0004(02)02126-6 | PubMed
9. **Warner JR,** Knopf PM, Rich A (1963) A multiple ribosomal structure in protein synthesis. *Proc Natl Acad Sci U S A* **49**:122-9 https://doi.org/10.1073/pnas.49.1.122 | PubMed
10. **Heiman M,** Kulicke R, Fenster RJ, Greengard P, Heintz N (2014) Cell type-specific mRNA purification by translating ribosome affinity purification (TRAP). *Nat Protoc* **9**:1282-91 https://doi.org/10.1038/nprot.2014.085 | PubMed
11. **Heiman M,** Schaefer A, Gong S, Peterson JD, Day M, Ramsey KE, et al. (2008) A translational profiling approach for the molecular characterization of CNS cell types. *Cell* **135**:738-48 https://doi.org/10.1016/j.cell.2008.10.028 | PubMed
12. **Zhao J,** Qin B, Nikolay R, Spahn CMT, Zhang G (2019) Translatomics: The Global View of Translation. *Int J Mol Sci* **20** https://doi.org/10.3390/ijms20010212 | PubMed
13. **McLachlan IG,** Flavell SW (2019) Cell Type-specific mRNA Purification in Caenorhabditis elegans via Translating Ribosome Affinity Purification. *Bio Protoc* **9**:e3328 https://doi.org/10.21769/bioprotoc.3328 | PubMed
14. **Schroeder DF,** McGhee JD (1998) Anterior-posterior patterning within the Caenorhabditis elegans endoderm. *Development* **125**:4877-87 https://doi.org/10.1242/dev.125.24.4877 | PubMed
15. **Beh CT,** Ferrari DC, Chung MA, McGhee JD (1991) An acid phosphatase as a biochemical marker for intestinal development in the nematode Caenorhabditis elegans. *Dev Biol* **147**:133-43 https://doi.org/10.1016/s0012-1606(05)80013-2 | PubMed
16. **Langfelder P,** Horvath S (2008) WGCNA: an R package for weighted correlation network analysis. *BMC Bioinformatics* **9**:559 https://doi.org/10.1186/1471-2105-9-559 | PubMed
17. **Higgins DP,** Weisman CM, Lui DS, D'Agostino FA, Walker AK (2022) Defining characteristics and conservation of poorly annotated genes in Caenorhabditis elegans using WormCat 2.0. *Genetics* **221** https://doi.org/10.1093/genetics/iyac085 | PubMed
18. **Holdorf AD,** Higgins DP, Hart AC, Boag PR, Pazour GJ, Walhout AJM, et al. (2020) WormCat: An Online Tool for Annotation and Visualization of Caenorhabditis elegans Genome-Scale Data. *Genetics* **214**:279-94 https://doi.org/10.1534/genetics.119.302919 | PubMed
19. **Ghaddar A,** Armingol E, Huynh C, Gevirtzman L, Lewis NE, Waterston R, et al. (2023) Whole-body gene expression atlas of an adult metazoan. *Sci Adv* **9**:eadg0506 https://doi.org/10.1126/sciadv.adg0506 | PubMed
20. **Ge SX,** Jung D, Yao R (2020) ShinyGO: a graphical gene-set enrichment tool for animals and plants. *Bioinformatics* **36**:2628-9 https://doi.org/10.1093/bioinformatics/btz931 | PubMed
21. **Mayer S,** Raulf MK, Lepenies B (2017) C-type lectins: their network and roles in pathogen recognition and immunity. *Histochem Cell Biol* **147**:223-37 https://doi.org/10.1007/s00418-016-1523-7 | PubMed
22. **Schulenburg H,** Hoeppner MP, Weiner J, Bornberg-Bauer E (2008) Specificity of the innate immune system and diversity of C-type lectin domain (CTLD) proteins in the nematode Caenorhabditis elegans. *Immunobiology* **213**:237-50 https://doi.org/10.1016/j.imbio.2007.12.004 | PubMed
23. **Pees B,** Yang W, Kloock A, Petersen C, Peters L, Fan L, et al. (2021) Effector and regulator: Diverse functions of C. elegans C-type lectin-like domain proteins. *PLoS Pathog* **17**:e1009454 https://doi.org/10.1371/journal.ppat.1009454 | PubMed
24. **Castaneda O,** Sotolongo V, Amor AM, Stocklin R, Anderson AJ, Harvey AL, et al. (1995) Characterization of a potassium channel toxin from the Caribbean Sea anemone Stichodactyla helianthus. *Toxicon* **33**:603-13 https://doi.org/10.1016/0041-0101(95)00013-c | PubMed
25. **Loukas A,** Hintz M, Linder D, Mullin NP, Parkinson J, Tetteh KK, et al. (2000) A family of secreted mucins from the parasitic nematode Toxocara canis bears diverse mucin domains but shares similar flanking six-cysteine repeat motifs. *J Biol Chem* **275**:39600-7 https://doi.org/10.1074/jbc.m005632200

PubMed

26. **Chhabra S,** Chang SC, Nguyen HM, Huq R, Tanner MR, Londono LM, et al. (2014) Kv1.3 channel-blocking immunomodulatory peptides from parasitic worms: implications for autoimmune diseases. *FASEB J* **28**:3952-64 https://doi.org/10.1096/fj.14-251967 | PubMed

27. **Troemel ER,** Chu SW, Reinke V, Lee SS, Ausubel FM, Kim DH (2006) p38 MAPK regulates expression of immune response genes and contributes to longevity in C. elegans. *PLoS Genet* **2**:e183 https://doi.org/10.1371/journal.pgen.0020183 | PubMed

28. **Shivers RP,** Youngman MJ, Kim DH (2008) Transcriptional responses to pathogens in Caenorhabditis elegans. *Curr Opin Microbiol* **11**:251-6 https://doi.org/10.1016/j.mib.2008.05.014 | PubMed

29. **Radeke LJ,** Herman MA (2020) Identification and characterization of differentially expressed genes in Caenorhabditis elegans in response to pathogenic and nonpathogenic Stenotrophomonas maltophilia. *BMC Microbiol* **20**:170 https://doi.org/10.1186/s12866-020-01771-1 | PubMed

30. **Tan MW,** Mahajan-Miklos S, Ausubel FM (1999) Killing of Caenorhabditis elegans by Pseudomonas aeruginosa used to model mammalian bacterial pathogenesis. *Proc Natl Acad Sci U S A* **96**:715-20 https://doi.org/10.1073/pnas.96.2.715 | PubMed

31. **Tullet JM,** Araiz C, Sanders MJ, Au C, Benedetto A, Papatheodorou I, et al. (2014) DAF-16/FoxO directly regulates an atypical AMP-activated protein kinase gamma isoform to mediate the effects of insulin/IGF-1 signaling on aging in Caenorhabditis elegans. *PLoS Genet* **10**:e1004109 https://doi.org/10.1371/journal.pgen.1004109 | PubMed

32. **Leiser SF,** Miller H, Rossner R, Fletcher M, Leonard A, Primitivo M, et al. (2015) Cell nonautonomous activation of flavin-containing monooxygenase promotes longevity and health span. *Science* **350**:1375-8 https://doi.org/10.1126/science.aac9257 | PubMed

33. **Ziegler DM** (2002) An overview of the mechanism, substrate specificities, and structure of FMOs. *Drug Metab Rev* **34**:503-11 https://doi.org/10.1081/dmr-120005650 | PubMed

34. **Xiao W,** Wang RS, Handy DE, Loscalzo J (2018) NAD(H) and NADP(H) Redox Couples and Cellular Energy Metabolism. *Antioxid Redox Signal* **28**:251-72 https://doi.org/10.1089/ars.2017.7216 | PubMed

35. **Raizen D,** Song BM, Trojanowski N, You YJ (2012) Methods for measuring pharyngeal behaviors. *WormBook* 1-13 https://doi.org/10.1895/wormbook.1.154.1 | PubMed

36. **Fukushige T,** Hawkins MG, McGhee JD (1998) The GATA-factor elt-2 is essential for formation of the Caenorhabditis elegans intestine. *Dev Biol* **198**:286-302 https://doi.org/10.1016/s0012-1606(98)80006-7 | PubMed

37. **Samuel BS,** Rowedder H, Braendle C, Felix MA, Ruvkun G (2016) Caenorhabditis elegans responses to bacteria from its natural habitats. *Proc Natl Acad Sci U S A* **113**:E3941-9 https://doi.org/10.1073/pnas.1607183113 | PubMed

38. **Zaslaver A,** Liani I, Shtangel O, Ginzburg S, Yee L, Sternberg PW (2015) Hierarchical sparse coding in the sensory system of Caenorhabditis elegans. *Proc Natl Acad Sci U S A* **112**:1185-9 https://doi.org/10.1073/pnas.1423656112 | PubMed

39. **Bricker DK,** Taylor EB, Schell JC, Orsak T, Boutron A, Chen YC, et al. (2012) A mitochondrial pyruvate carrier required for pyruvate uptake in yeast, Drosophila, and humans. *Science* **337**:96-100 https://doi.org/10.1126/science.1218099 | PubMed

40. **Herzig S,** Raemy E, Montessuit S, Veuthey JL, Zamboni N, Westermann B, et al. (2012) Identification and functional expression of the mitochondrial pyruvate carrier. *Science* **337**:93-6 https://doi.org/10.1126/science.1218530 | PubMed

41. **Gray LR,** Tompkins SC, Taylor EB (2014) Regulation of pyruvate metabolism and human disease. *Cell Mol Life Sci* **71**:2577-604 https://doi.org/10.1007/s00018-013-1539-2 | PubMed

42. **Hickey JW,** Becker WR, Nevins SA, Horning A, Perez AE, Zhu C, et al. (2023) Organization of the human intestine at single-cell resolution. *Nature* **619**:572-84 https://doi.org/10.1038/s41586-023-05915-x | PubMed

43. **Bakar R Bany,** Reimann F, Gribble FM (2023) The intestine as an endocrine organ and the role of gut hormones in metabolic regulation. *Nat Rev Gastroenterol Hepatol* **20**:784-96 https://doi.org/10.1038/s41575-023-00830-y | PubMed

44. **Zietek T,** Rath E (2016) Inflammation Meets Metabolic Disease: Gut Feeling Mediated by GLP-1. *Front Immunol* **7**:154 https://doi.org/10.3389/fimmu.2016.00154 | PubMed

45. **Mahoney TR,** Luo S, Round EK, Brauner M, Gottschalk A, Thomas JH, et al. (2008) Intestinal signaling to GABAergic neurons regulates a rhythmic behavior in Caenorhabditis elegans. *Proc Natl Acad Sci U S A* **105**:16350-5 https://doi.org/10.1073/pnas.0803617105 | PubMed

46. **Beg AA,** Ernstrom GG, Nix P, Davis MW, Jorgensen EM (2008) Protons act as a transmitter for muscle contraction in C. elegans. *Cell* **132**:149-60 https://doi.org/10.1016/j.cell.2007.10.058 | PubMed

47. **Gt Borgonie,** Claeys M, Waele DD, Coomans A (1995) In-vivo and in-vitro characterization of the intestine of fifteen bacteriophagous nematodes (Nematoda: Rhabditida). *Fundamental and applied nematology* **18**:115-22

48. **Borgonie G,** Claeys M, Dewaele D, Coomans A (1995) Ultrastructure of the Intestine of the Bacteriophagous Nematodes Caenorhabditis-Elegans, Panagrolaimus Superbus and Acrobeloides Maximus (Nematoda, Rhabditida). *Fundamental and Applied Nematology* **18**:123-33

49. **Panek J,** Gang SS, Reddy KC, Luallen RJ, Fulzele A, Bennett EJ, et al. (2020) A cullin-RING ubiquitin ligase promotes thermotolerance as part of the intracellular pathogen response in Caenorhabditis elegans. *Proc Natl Acad Sci U S A* **117**:7950-60 https://doi.org/10.1073/pnas.1918417117 | PubMed

50. **Martinez-Reyes I,** Chandel NS (2020) Mitochondrial TCA cycle metabolites control physiology and disease. *Nat Commun* **11**:102 https://doi.org/10.1038/s41467-019-13668-3 | PubMed

51. **Picard M,** Shirihai OS (2022) Mitochondrial signal transduction. *Cell Metab* **34**:1620-53 https://doi.org/10.1016/j.cmet.2022.10.008 | PubMed

52. **Nargund AM,** Fiorese CJ, Pellegrino MW, Deng P, Haynes CM (2015) Mitochondrial and nuclear accumulation of the transcription factor ATFS-1 promotes OXPHOS recovery during the UPR(mt). *Mol Cell* **58**:123-33 https://doi.org/10.1016/j.molcel.2015.02.008 | PubMed

53. **Behr S,** Brameyer S, Witting M, Schmitt-Kopplin P, Jung K (2017) Comparative analysis of LytS/LytTR-type histidine kinase/response regulator systems in gamma-proteobacteria. *PLoS One* **12**:e0182993 https://doi.org/10.1371/journal.pone.0182993 | PubMed

54. **Fried L,** Behr S, Jung K (2013) Identification of a target gene and activating stimulus for the YpdA/YpdB histidine kinase/response regulator system in Escherichia coli. *J Bacteriol* **195**:807-15 https://doi.org/10.1128/jb.02051-12 | PubMed

55. **Paczia N,** Nilgen A, Lehmann T, Gatgens J, Wiechert W, Noack S (2012) Extensive exometabolome analysis reveals extended overflow metabolism in various microorganisms. *Microb Cell Fact* **11**:122 https://doi.org/10.1186/1475-2859-11-122 | PubMed

56. **Yasid NA,** Rolfe MD, Green J, Williamson MP (2016) Homeostasis of metabolites in Escherichia coli on transition from anaerobic to aerobic conditions and the transient secretion of pyruvate. *R Soc Open Sci* **3**:160187 https://doi.org/10.1098/rsos.160187 | PubMed

57. **Zhang Y,** Chou JH, Bradley J, Bargmann CI, Zinn K (1997) The Caenorhabditis elegans seven-transmembrane protein ODR-10 functions as an odorant receptor in mammalian cells. *Proc Natl Acad Sci U S A* **94**:12162-7 https://doi.org/10.1073/pnas.94.22.12162 | PubMed

58. **Harvald EB,** Sprenger RR, Dall KB, Ejsing CS, Nielsen R, Mandrup S, et al. (2017) Multi-omics Analyses of Starvation Responses Reveal a Central Role for Lipoprotein Metabolism in Acute Starvation Survival in C. elegans. *Cell Syst* **5**:38-52 e4 https://doi.org/10.1016/j.cels.2017.06.004 | PubMed

59. **Maier T,** Guell M, Serrano L (2009) Correlation of mRNA and protein in complex biological samples. *FEBS Lett* **583**:3966-73 https://doi.org/10.1016/j.febslet.2009.10.036 | PubMed

60. **Vogel C,** Marcotte EM (2012) Insights into the regulation of protein abundance from proteomic and transcriptomic analyses. *Nat Rev Genet* **13**:227-32 https://doi.org/10.1038/nrg3185 | PubMed

61. **Thomas A,** Lee PJ, Dalton JE, Nomie KJ, Stoica L, Costa-Mattioli M, et al. (2012) A versatile method for cell-specific profiling of translated mRNAs in Drosophila. *PLoS One* **7**:e40276 https://doi.org/10.1371/journal.pone.0040276 | PubMed

62. **Huang Y,** Ainsley JA, Reijmers LG, Jackson FR (2013) Translational profiling of clock cells reveals circadianly synchronized protein synthesis. *PLoS Biol* **11**:e1001703 https://doi.org/10.1371/journal.pbio.1001703 | PubMed

63. **Zhang KX,** Tan L, Pellegrini M, Zipursky SL, McEwen JM (2016) Rapid Changes in the Translatome during the Conversion of Growth Cones to Synaptic Terminals. *Cell Rep* **14**:1258-71 https://doi.org/10.1016/j.celrep.2015.12.102 | PubMed

64. **Gracida X,** Calarco JA (2017) Cell type-specific transcriptome profiling in C. elegans using the Translating Ribosome Affinity Purification technique. *Methods* **126**:130-7 https://doi.org/10.1016/j.ymeth.2017.06.023 | PubMed

65. **Sanz E,** Yang L, Su T, Morris DR, McKnight GS, Amieux PS (2009) Cell-type-specific isolation of ribosome-associated mRNA from complex tissues. *Proc Natl Acad Sci U S A* **106**:13939-44 https://doi.org/10.1073/pnas.0907143106 | PubMed

66. **Wester LE,** Lanjuin A, Bruckisch EHW, Perez-Matos MC, Stine PG, Heintz C, et al. (2023) A single-copy knockin translating ribosome immunoprecipitation toolkit for tissue-specific profiling of actively translated mRNAs in C. elegans. *Cell Rep Methods* **3**:100433 https://doi.org/10.1016/j.crmeth.2023.100433 | PubMed

67. **Rhoades JL,** Nelson JC, Nwabudike I, Yu SK, McLachlan IG, Madan GK, et al. (2019) ASICs Mediate Food Responses in an Enteric Serotonergic Neuron that Controls Foraging Behaviors. *Cell* **176**:85-97 e14 https://doi.org/10.1016/j.cell.2018.11.023 | PubMed

68. **Gracida X,** Dion MF, Harris G, Zhang Y, Calarco JA (2017) An Elongin-Cullin-SOCS Box Complex Regulates Stress-Induced Serotonergic Neuromodulation. *Cell Rep* **21**:3089-101 https://doi.org/10.1016/j.celrep.2017.11.042 | PubMed

69. **Koterniak B,** Pilaka PP, Gracida X, Schneider LM, Pritisanac I, Zhang Y, et al. (2020) Global regulatory features of alternative splicing across tissues and within the nervous system of C. elegans. *Genome Res* **30**:1766-80 https://doi.org/10.1101/gr.267328.120 | PubMed

70. **Nousch M** (2020) RPL-4 and RPL-9 Mediated Ribosome Purifications Facilitate the Efficient Analysis of Gene Expression in Caenorhabditis elegans Germ Cells. *G3 (Bethesda)* **10**:4063-9 https://doi.org/10.1534/g3.120.401644 | PubMed

71. **Shi Z,** Fujii K, Kovary KM, Genuth NR, Rost HL, Teruel MN, et al. (2017) Heterogeneous Ribosomes Preferentially Translate Distinct Subpools of mRNAs Genome-wide. *Mol Cell* **67**:71-83 e7 https://doi.org/10.1016/j.molcel.2017.05.021 | PubMed

72. **Brenner S** (1974) The genetics of Caenorhabditis elegans. *Genetics* **77**:71-94 https://doi.org/10.1093/genetics/77.1.71 | PubMed

73. **Noble T,** Stieglitz J, Srinivasan S (2013) An integrated serotonin and octopamine neuronal circuit directs the release of an endocrine signal to control C. elegans body fat. *Cell Metab* **18**:672-84 https://doi.org/10.1016/j.cmet.2013.09.007 | PubMed

74. **Palamiuc L,** Noble T, Witham E, Ratanpal H, Vaughan M, Srinivasan S (2017) A tachykinin-like neuroendocrine signalling axis couples central serotonin action and nutrient sensing with peripheral lipid metabolism. *Nat Commun* **8**:14237 https://doi.org/10.1038/ncomms14237 | PubMed

75. **Kamath RS,** Ahringer J (2003) Genome-wide RNAi screening in Caenorhabditis elegans. *Methods* **30**:313-21 https://doi.org/10.1016/s1046-2023(03)00050-1 | PubMed

76. **Srinivasan S,** Sadegh L, Elle IC, Christensen AG, Faergeman NJ, Ashrafi K (2008) Serotonin regulates C. elegans fat and feeding through independent molecular mechanisms. *Cell Metab* **7**:533-44 https://doi.org/10.1016/j.cmet.2008.04.012 | PubMed

77. **Filipowicz A,** Lalsiamthara J, Aballay A (2022) Dissection of a sensorimotor circuit underlying pathogen aversion in C. elegans. *BMC Biol* **20**:229 https://doi.org/10.1186/s12915-022-01424-x | PubMed

78. **Dobin A,** Davis CA, Schlesinger F, Drenkow J, Zaleski C, Jha S, et al. (2013) STAR: ultrafast universal RNA-seq aligner. *Bioinformatics* **29**:15-21 https://doi.org/10.1093/bioinformatics/bts635 | PubMed

79. **Liao Y,** Smyth GK, Shi W (2014) featureCounts: an efficient general purpose program for assigning sequence reads to genomic features. *Bioinformatics* **30**:923-30 https://doi.org/10.1093/bioinformatics/btt656 | PubMed

80. **Andrews S** (2010) FastQC: A Quality Control Tool for High Throughput Sequence Data. http://www.bioinformatics.babraham.ac.uk/projects/fastqc/

81. **Love MI,** Huber W, Anders S (2014) Moderated estimation of fold change and dispersion for RNA-seq data with DESeq2. *Genome Biol* **15**:550 https://doi.org/10.1186/s13059-014-0550-8 | PubMed

82. **Wu T,** Hu E, Xu S, Chen M, Guo P, Dai Z, et al. (2021) clusterProfiler 4.0: A universal enrichment tool for interpreting omics data. *Innovation* **2**:100141 https://doi.org/10.1016/j.xinn.2021.100141 | PubMed

Liu CC, Seban N, Srinivasan S (2026) Ribo-TRAPseq identifies spacially distinct roles for the anterior and posterior intestine for metabolic regulation in C. elegans. NCBI Gene Expression Omnibus. ID GSE306302 https://www.ncbi.nlm.nih.gov/geo/query/acc.cgi?acc=GSE306302

Peer reviews

Reviewer #1 (Public review):

Summary

In this study, the authors have performed tissue-specific ribosome pulldown to identify gene expression (translatome) differences in the anterior vs posterior cells of the C. elegans intestine. They have performed this analysis in fed and fasted states of the animal. The data generated will be very useful to the C. elegans community, and the role of pyruvate shown in this study will result in interesting follow-up investigations.

However, several strong claims made in the study are solely based on in silico predictions and are not supported by experimental evidence.

Comments on revised version.

The authors have been responsive to the comments, but have not added new experiments in this manuscript that would have clarified and improved some of the mentioned shortcomings of the study.

There are 3 comments that the authors should address:

(1) In their response to reviewers, the authors agree that "the Pges-1deltaB promoter is not absolutely restricted to INT1 and that weak GFP expression can also be detected in INT2." They also mention that "because Pges-1deltaB is an engineered promoter derived from the intestine-specific Pges-1 promoter, this low-level INT2 expression is not unexpected." However, in line 93 of the revised manuscript, the authors claim that "Pges-1deltaB is strictly expressed in INT1 cells". This discrepancy should be fixed. They should instead describe this in line 93 as "Pges-1deltaB expression is very strongly enriched in INT1 cells, but low-level expression in INT2 was also detected".

(2) In response to reviewers, the authors explained that "Our model is that fasting induces INS-7 secretion by lowering intracellular pyruvate in INT1 cells. Under this framework, blocking mitochondrial pyruvate breakdown would be expected to reduce pyruvate utilization and thus maintain intracellular pyruvate, preventing the drop in pyruvate that

normally occurs during fasting. This would explain why these manipulations suppress fasting-induced INS-7 secretion." However, the effect of blocking import of pyruvate from cytosol into mitochondria (via knockdown of mitochondrial pyruvate carrier genes mpc-1 and mpc-2) does not agree with their proposed model. Blocking mitochondrial import of pyruvate should maintain cytosolic pyruvate levels and thus prevent the drop in pyruvate that normally occurs during fasting. In such a scenario, we would expect to see no increase in INS-7 secretion during fasting, which is opposite to the result in Fig.7D. If the pyruvate sensor is in the cytosol, we would expect that the mpc-1/2 RNAi treated animals would be unable to increase INS-7 secretion upon starvation. If the pyruvate sensor is in the mitochondrial matrix, we would expect that the mpc-1/2 RNAi treated animals would have higher INS-7 secretion than vector RNAi control animals in fed conditions. How do the authors explain this discrepancy between their observed results and their proposed model? Why does blocking mitochondrial import of pyruvate affect only refeeding-induced reduction in INS-7 secretion but not fasting-induced increase in INS-7 secretion? Is it possible that instead of responding to absolute intracellular concentrations of pyruvate, the pyruvate sensor increases INS-7 secretion upon detecting a relative drop in the mitochondrial levels of pyruvate (or its downstream metabolite)? This should be described in the text to better interpret the mpc-1/2 RNAi results.

(3) Line 493: The authors refer to 'Table S4', which is not included in the manuscript.

https://doi.org/10.7554/eLife.109237.2.sa2

Reviewer #3 (Public review):

In this study, Liu and colleagues utilize TRAP-seq to profile the repertoire of actively translated mRNAs in different intestinal cell types (anterior INT1 vs. posterior INT2-9 cells) in C. elegans. A key goal of this study was to identify transcripts differentially expressed/translated between these intestinal cell subtypes in the context of animals being well fed or subjected to acute (30 minutes) or chronic (3 hours) starvation, followed by refeeding.

The authors identify a number of differentially expressed genes across all of the conditions tested. They then provide an initial survey of the landscape of translatome changes through Weighted Gene Network Correlation Analysis (WGNA), and some high-level functional surveys via Gene Ontology (GO) term analysis and protein domain analysis. The authors validate the enriched expression patterns of some of their identified candidate genes using fluorescent promoter fusion reporters, confirming INT1-specific expression. The authors further implicate the role of several other candidate genes in pathogen avoidance and in response to nutritional cues by knocking them down specifically in INT1 cells by RNAi. Finally, the authors identify pyruvate as a major nutrient signal coming from the bacterial diet that suppresses the release of a key insulin peptide (INS-7) and identify some of the genes expressed in INT1 that are required for this response.

Strengths:

(1) Good use of and justification for TRAP-seq, because scRNA-seq would be difficult under the varied conditions used (starvation, refeeding)

(2) The manuscript is generally clear to read, and the data are generally well-presented with good supporting data that includes replicates, sample sizes, error measurements, and associated statistics.

(3) The dataset will be an interesting resource to mine for future studies focusing on mechanisms of how particular intestinal cell types respond to different environmental signals.

Weaknesses:

(1) A limitation of TRAP-seq, although powerful, is that only relative comparisons can be made between genotypes/conditions to identify differentially-expressed genes, rather than assessing whether a given gene is expressed at a certain level in a cell type under a certain condition. This limitation is due to the non-specific association of sticky RNA species to the beads during the immunoprecipitation step. This is a minor point however, and the authors do a nice job of focusing their analysis on differentially expressed transcripts in the current study.

(2) Another limitation of the current study is that the experiments testing the role of candidate genes identified by their profiling experiments do not dive a bit deeper into providing a mechanistic understanding of the phenotypes being studied. At present, the results are thus viewed more as a genomics-based screen with some limited follow-up on interesting hits. However, this reviewer appreciates that when placed in context of the work presented, a presentation of the profiling data along with some validation is an excellent starting point for future mechanistic studies elaborating on these interesting candidates.

Appraisal of whether the authors achieved their aims, and whether the results support their conclusions.

The main goal of the study was to survey the dynamic responses at the level of actively translated mRNAs of the INT1 vs INT2-9 cells in response to metabolic challenge.

Overall, the authors use established methods to perform their genome-wide analysis, and the set of differentially regulated genes are enriched for expected molecular functions and form coherent networks in anticipated pathways.

The validation experiments (promoter::GFP fusion reporters, INT1-specific knockdowns of highly regulated genes) further corroborate the quality of the TRAP-seq datasets generated.

I have a few points for the authors that would further strengthen this work:

(1) The authors rightfully focus on the top differentially-regulated candidates, but it's unclear at present how far down their fold change list would lead to expression pattern validations. It would be useful to test a few more promoter::GFP fusion reporters at different enrichment/fold-change/statistical cutoffs.

(2) Although the INT1-specific RNAi provides a convenient strategy for rapidly perturbing and testing genes of interest for phenotypes, independently validating the knockdowns with genetic mutants, or alternatively (if genes are essential), degron alleles.

Likely impact of the work on the field, and the utility of the methods and data to the community.

The TRAP-seq data and list of differentially-expressed candidate genes will form an interesting set of high-priority candidates to study for their role in the reception and transduction of nutritional cues in response to food status and pathogens. This data will thus benefit the C. elegans community of researchers studying the mechanisms governing these phenomena.

Comments on revised version:

I think the authors have done a good job of addressing the suggestions from the previous round of review in this new version.

https://doi.org/10.7554/eLife.109237.2.sa1

Author response:

The following is the authors' response to the original reviews.

Public Reviews:

Reviewer #1 (Public review):

Summary

In this study, the authors have performed tissue-specific ribosome pulldown to identify gene expression (translatome) differences in the anterior vs posterior cells of the C. elegans intestine. They have performed this analysis in fed and fasted states of the animal. The data generated will be very useful to the C. elegans community, and the role of pyruvate shown in this study will result in interesting follow-up investigations.

However, several strong claims made in the study are solely based on in silico predictions and are not supported by experimental evidence.

Strengths:

Several studies in the past have predicted different functions of the anterior (INT1) vs posterior (INT2-9) epithelial cells of the C. elegans intestine based on their anatomy and ultrastructure, but detailed characterization of differences in gene expression between these cell types (and whether indeed these are different 'cell types') was lacking prior to this study. The genes and drivers identified to be exclusively expressed in the anterior vs posterior segments of the intestine will be very helpful to selectively modulate different parts of the C. elegans intestine in future studies.

Another strength of this study is the careful experimental design to test how the anterior vs posterior cell types of the intestine respond differently to food deprivation and recovery after return to food. These comparisons between 'states' of a cell in different physiological conditions are difficult to pick up in single-cell analyses due to low sequencing depth, which can fail to identify subtle modulation of gene expression.

The TRAP-associated bulk RNA-seq approach used in this study is more suitable for such comparisons and provides additional information on post-transcriptional regulation during metabolic stress.

A key finding of this study is that pyruvate levels modulate the translation state of anterior intestinal cells during fasting. Characterization of pyruvate metabolism genes, especially of the enzymes involved in its mitochondrial breakdown, provides novel insights into how gut epithelial cells respond to the acute absence of food.

Weaknesses:

Unlike previous TRAP-seq studies (PMID: 30580965, 36044259, 36977417) that reported sequencing data for both input and IP samples, this study only reports the sequencing data for IP samples. Since biochemical pulldowns are variable across replicates, it is difficult to know if the observed differences between different conditions are due to biological factors or differences in IP efficiency. More importantly, since two different TRAP lines were utilized in this study and a large proportion of the results focus on the differences between the translational profiles of INT1 vs INT2-9 cells, it is essential to know if the IP worked with similar efficiency for both TRAP strains that likely have different expression levels of the HA-tagged ribosomal protein. One way to estimate this would be to perform qRT-PCR of genes that are known to be enriched in all intestinal cells and determine whether their fold-enrichment over housekeeping genes (normalized to

> *input) is similar in INT1 vs INT2-9 TRAP strains and across the fed vs fasted conditions. The authors, in fact, mention variability across biological replicates, due to which certain replicates were excluded from their WGCNA analysis.*

We appreciate the reviewer's comments. We agree that the lack of matched input sequencing libraries limits our ability to directly assess IP efficiency across replicates, conditions, and TRAP strains. However, several features of the dataset support the conclusion that the major differences reported here reflect biological rather than purely technical variation. First, the RPL-22-3xHA construct was integrated into each line to improve consistency across experiments. Second, although the INT2-9 TRAP strain yielded more RNA than the INT1 strain, as expected given the larger number of labeled cells, downstream analyses were performed on normalized count data rather than raw counts. Third, principal component analysis showed robust separation by promoter identity across all conditions, and expected INT1-enriched genes such as *ins-7* were recovered in the INT1 dataset. Together, these observations support the interpretation that the TRAP datasets capture reproducible, cell-type-specific differences in ribosome-associated transcripts. Nonetheless, we agree that direct input-normalized measurements would further strengthen the study, and we will explicitly note this as an important limitation.

> *It appears that GFP expression is also detectable in INT2 (in addition to strong expression in INT1 in Fig.1A). Compared to INT3-9, which looks red, INT2 cells appear yellow, suggesting that the expression patterns of the two TRAP drivers are not mutually exclusive, which changes the interpretation of many of the results described in the study.*

We agree that the *Pges-1ΔB* promoter is not absolutely restricted to INT1 and that weak GFP expression can also be detected in INT2. Because *Pges-1ΔB* is an engineered promoter derived from the intestine-specific *Pges-11* promoter, this low-level INT2 expression is not unexpected. However, we note that the expression level in INT1 is substantially higher than in INT2. Thus, although the expression patterns of the two TRAP drivers are not completely mutually exclusive, *Pges-1ΔB* still provides the most selective available tool for enriching the INT1 translatome in the context of the current study.

> *Some parts of the study overemphasize the differences between the INT1 vs INT2-9 cell types, which is a biased representation of the results. For example, the authors specifically point out that 270 genes are differentially expressed in opposite directions in INT1 vs INT2-9 cell types during acute (30 min) fasting without mentioning the 1,268 genes that are differentially expressed in the same direction. They also do not mention here that 96% of the genes are differentially expressed in the same direction in INT1 and INT2-9 cell types after prolonged (180 min) fasting, suggesting that the divergent translational responses of these cell types are only observed in the first 30 minutes of food deprivation. Similar results have also been reported for the effect of fasting on locomotory and feeding behaviors, where 30 min of fasting produces more variable effects, which become more consistent after longer periods of fasting (PMID: 36083280). Hence, the effects of brief food deprivation should be interpreted with caution.*

The intestine functions as a discrete and cohesive organ, so the expected result is that there would be no differences across the different cell types. For us, the surprise was that, in fact, there are differences between these cells at all. However, the point is well taken, and we have added a statement in the text to reflect that many genes change similarly in INT1 and INT2-9, while the differences reflect important functional divergence between these cell types.

> *Many of the interpretations of this study primarily rely on pathway enrichment analyses, which are based on the known function of genes. The function of uncharacterized genes that were found to be differentially expressed in INT1 vs INT2-9 cell types, e.g., the ShKT proteins, was not explored in this study. In addition, overreliance on pathway enrichment tools (instead of functional validation) has resulted in several conflicting findings. For*

> *example, one of the main messages of this study is that INT1 cells specialize in immune and stress response in response to fasting, which relies on pathway analysis in Figs 5E and 5F. However, pathway analysis at a different time point (shown in Figure S5A) indicates that INT2-9 cells show a much stronger increase in translation of stress and pathogen-responsive genes compared to INT1 cells. Hence, some of the results should be interpreted as different translational effects in INT1 vs INT2-9 cells after different lengths of food deprivation, without making broad claims about selective pathways being affected only in specific cell types.*

We agree that some interpretations in the manuscript relied heavily on pathway enrichment analyses and should be stated more cautiously. In particular, we agree that the current data are most consistent with state-dependent differences in translational responses between INT1 and INT2-9 cells across different durations of food deprivation, rather than with the strongest version of a claim that specific pathways are selectively engaged only in one intestinal subset. We also agree that uncharacterized genes, including the ShKT family, were not mechanistically explored in the present study and should be presented as important candidates for future investigation.

> *The authors have compared their TRAP-seq results with genes enriched in the anterior and posterior intestine clusters from a previously published whole-animal adult scRNA dataset (PMID: 37352352). They claim that their TRAP-seq results are in agreement with the findings of the scRNA study. However, among the 10 genes from the 'posterior intestine' scRNA cluster in Fig.S1E, six are downregulated in the INT1 vs INT2-9 comparison, while four are upregulated. Hence, there is no clear agreement between the two studies in terms of the top enriched genes in the anterior vs posterior intestine, which should be considered for cross-study comparisons in the future.*

We have removed the original Figure S1C–E, replacing it with a more informative analysis. The genes in the original panel were drawn from the top markers reported for intestinal clusters in Ghaddar et al. (PMID: 37352352). However, these markers were defined by comparison with all *C. elegans* cell types, rather than by comparisons among anterior, middle, and posterior intestinal populations, and are therefore not optimal for resolving differences between intestinal subregions. We instead assessed the expression levels of our INT1 up-regulated genes in their intestinal cluster and found that they have higher expression in the anterior intestine cluster (new Figure S1C). These results underscore the strength of our dataset for identifying genes that distinguish INT1 from INT2–9.

> *The authors describe in the manuscript that they have performed INT1-specific RNAi for two C-type lectin genes that are upregulated during fasting. Due to a recent expansion of C-type lectin genes in C. elegans, there is a high chance of off-target effects of RNAi that is designed for members of this gene family. More trustworthy results could have been obtained using CRISPR-based loss-of-function alleles for these genes, one of which is publicly available. Also, the authors do not provide any explanation for why knockdown of these stress-response genes, which are activated in INT1 cells in response to food deprivation, results in improved resistance to pathogens. This, in fact, suggests a role of INT1 cells in increasing pathogen susceptibility, and not pathogen resistance, during food deprivation.*

We agree that RNAi targeting C-type lectin family members may be susceptible to off-target effects, and that validation with CRISPR null alleles, where available, would strengthen these findings. In the current study, we used INT1-specific RNAi as a cell-specific first-pass approach to test candidate gene function. We also agree that the pathogen phenotype requires cautious interpretation. Specifically, the finding that knockdown of fasting-induced INT1 lectin genes improves pathogen resistance does not support a simple protective model for these genes. Instead, it suggests that INT1-expressed stress-response genes modulate host susceptibility or host-pathogen interactions.

> *Many of the studies in this field (e.g., references 2-4 in this article) have investigated the effects of food deprivation ranging from 4 hr to 24 hr, which results in activation of starvation responses in C. elegans. In contrast, the authors have used shorter time periods of fasting (30 min and 180 min), and most of their follow-up experiments have used 30 min of food deprivation. Previous work has shown that the effects of food deprivation can either accumulate over time (i.e., the effect gets stronger with longer food deprivation) or can be transient (i.e., only observed briefly after removal of food and not observed during long-term food deprivation). Starvation-induced transcription factors such as DAF-16/FoxO and HLH-30 show strong translocation to the nucleus only after 30 min of fasting. Though gene expression changes in all stages of food deprivation are of biological relevance, the authors have missed the opportunity to explore whether increased INS-7 secretion from the anterior intestine is dependent on these starvation-induced transcription factors (which can be easily tested using loss-of-function alleles) or is due to other fast-acting regulatory mechanisms induced due to the absence of food contents in the gut lumen. A previous study (PMID: 40991693) has shown that DAF-16 activation during prolonged starvation shuts down insulin peptide secretion from the intestinal epithelial cells. Hence, it is not clear if increased INS-7 secretion is only a feature of short-term food deprivation or is also a signature of long-term starvation (e.g., at 8 hr or 16 hr timepoints). Since most of the INS-7 secretion data in this study are for 30 min of fasting, it remains unknown whether the discovered regulators of INS-7 secretion can be generalized for extended food deprivation that triggers major metabolic changes, such as fat loss (e.g., conditions shown in Figure 1D).*

We agree that short-term food deprivation and prolonged starvation likely engage distinct regulatory mechanisms, and that our study primarily addresses an early phase of food deprivation rather than the full spectrum of starvation responses described in prior work. We selected the 30 min fasting condition because our previous study showed that INS-7 secretion is induced within this interval and returns to baseline upon refeeding, even before detectable intestinal fat loss. We also included a 180 min fasting condition to capture a later state associated with metabolic changes. However, we agree that the present study does not determine whether the regulators of INS-7 secretion identified here also govern secretion during more prolonged starvation (for example, 8 hr or 16 hr), nor does it test whether starvation-responsive transcription factors such as DAF-16 or HLH-30 contribute to this regulation. We appreciate that determining how this response transitions during prolonged starvation will be an important direction for future work.

> *Two previous studies (PMID: 18025456, 40991693) have shown a strong reduction in the expression of ins-7 in the anterior intestine using GFP-based reporters (both promoter fusions and endogenous CRISPR-generated) and in whole-animal RNA-seq data from starved animals. These results are in contrast to the increased INS-7 secretion from INT1 cells during fasting that is reported in this study. The authors here have reported that INS-7 translation is higher in INT1 compared to INT2-9 during fed, acute fasted, and chronic fasted conditions, but they have not shown whether INS-7 translation is upregulated during acute and chronic fasting in INT1 cells in their TRAP-seq analysis. Knowing whether increased INS-7 secretion during acute fasting is due to increased*

> *transcription, translation, or secretion of INS-7 is crucial to resolve the discrepancy between these studies.*

In our dataset, INS-7 translation in INT1 tended to increase during acute fasting relative to the fed state ($log_2FC = 0.69$), although this effect did not reach statistical significance after adjustment for multiple comparisons. Consistent with this trend, our secretion assay showed that INS-7 release from INT1 increases during fasting. However, we agree that the current data do not distinguish whether this increase in secretion is driven by enhanced synthesis, regulated release of pre-existing peptide stores, or a combination of both.

> ***Reviewer #2 (Public review):***
>
> *Summary:*
>
> *In this study, the authors set out to understand whether the discrete segments of the C.elegans intestine were specialized to carry out distinct functions during an animal's exposure and adaptation to a fast-changing nutrient environment. To achieve this, the authors used a method called Translating ribosome affinity purification (TRAP), which provides a snapshot of what genes are being translated into proteins (and therefore functionally prioritized by the animal) under different fasting and re-feeding conditions. By expressing the TRAP constructs in two distinct segments of the intestine (INT1) and (INT2-9), the authors were able to identify how these segments responded to changing nutrient availability.*
>
> *Already under steady state nutrient conditions, the authors found that INT1 and INT2-9 appeared to have different 'tasks', with INT1 expressing more immune- and stress-response related genes. Exposing animals to different regimens of starvation and refeeding also showed marked differences between the intestinal segments, and the gene expression patterns in INT1 were consistent with INT1 cells playing an integrative role in linking nutrient cues to the secretion of insulin molecules that regulate fat metabolism with food intake. In summary, the data presented catalogue, for the first time, gene expression differences between two areas of the intestine, suspected to play different roles, and through clever experiments, links these gene expression changes to responses to nutrient availability.*
>
> *Strengths:*
>
> *The data presented catalogue - for the first time and in a careful manner - gene expression differences between two areas of the intestine. They strongly support the presence of intriguing differences between two areas of the intestine in immune, metabolic, and stress-response regulation, and link these gene expression changes to the responses of these regions to nutrient availability.*
>
> *Weaknesses:*
>
> *The conclusions of this paper are mostly well-supported by data, but the relevance of the changing gene expression patterns could be better clarified and extended in the discussion.*

We thank the reviewer for this constructive comment. In the revised manuscript, we have now expanded the discussion to more clearly interpret these dynamic translatomic changes in the context of intestinal subset specialization. The most pronounced difference between INT1 and INT2-9 cells is the enrichment of stress-response genes in INT1. Based on the present findings, together with our previous work identifying INS-7 as an INT1-secreted signal (PMID: 39127676), we propose that INT1 cells are sentinel enteroendocrine cells that integrate information from the luminal environment and the metabolic state of intestinal cells.

Reviewer #3 (Public review):

Summary:

In this study, Liu and colleagues utilize TRAP-seq to profile the repertoire of actively translated mRNAs in different intestinal cell types (anterior INT1 vs. posterior INT2-9 cells) in C. elegans. A key goal of this study was to identify transcripts differentially expressed/translated between these intestinal cell subtypes in the context of animals being well fed or subjected to acute (30 minutes) or chronic (3 hours) starvation, followed by refeeding.

The authors identify a number of differentially expressed genes across all of the conditions tested. They then provide an initial survey of the landscape of translatome changes through Weighted Gene Network Correlation Analysis (WGNA), and some high-level functional surveys via Gene Ontology (GO) term analysis and protein domain analysis. The authors validate the enriched expression patterns of some of their identified candidate genes using fluorescent promoter fusion reporters, confirming INT1-specific expression. The authors further implicate the role of several other candidate genes in pathogen avoidance and in response to nutritional cues by knocking them down specifically in INT1 cells by RNAi. Finally, the authors identify pyruvate as a major nutrient signal coming from the bacterial diet that suppresses the release of a key insulin peptide (INS-7), and identify some of the genes expressed in INT1 that are required for this response.

Strengths:

(1) Good use of and justification for TRAP-seq, because scRNA-seq would be difficult under the varied conditions used (starvation, refeeding).

(2) The manuscript is generally clear to read, and the data are generally well-presented with good supporting data that includes replicates, sample sizes, error measurements, and associated statistics.

(3) The dataset will be an interesting resource to mine for future studies focusing on mechanisms of how particular intestinal cell types respond to different environmental signals.

Weaknesses:

(1) A limitation of TRAP-seq, although powerful, is that only relative comparisons can be made between genotypes/conditions to identify differentially-expressed genes, rather than assessing whether a given gene is expressed at a certain level in a cell type under a certain condition. This limitation is due to the non-specific association of sticky RNA species with the beads during the immunoprecipitation step. This is a minor point, however, and the authors do a nice job of focusing their analysis on differentially expressed transcripts in the current study.

We agree that a limitation of TRAP-seq is that it is best suited for relative comparisons across cell types or conditions, rather than for determining the absolute expression level of a given transcript in a specific cell type. As the reviewer notes, this limitation arises in part from nonspecific recovery of background or sticky RNAs during the immunoprecipitation step, complicating the interpretation of absolute expression levels. For this reason, our analysis was designed to focus primarily on differentially enriched transcripts between INT1 and INT2-9 cells and across feeding states, rather than on assigning absolute expression levels to individual genes. We appreciate the reviewer's recognition of this point. Our study uses

TRAP-seq specifically to define relative translatomic differences between intestinal subsets and physiological states, which is well aligned with the strengths of this approach.

> *(2) Another limitation of the current study is that the experiments testing the role of candidate genes identified by their profiling experiments do not delve a bit deeper into providing a mechanistic understanding of the phenotypes being studied. At present, the results are thus viewed more as a genomics-based screen with some limited follow-up on interesting hits. However, this reviewer appreciates that when placed in the context of the work presented, a presentation of the profiling data along with some validation is an excellent starting point for future mechanistic studies elaborating on these interesting candidates.*

We agree that the current study does not fully resolve the molecular mechanisms by which the candidate genes identified by TRAP-seq regulate the phenotypes examined here. Our primary goal was to generate a spatially resolved translatomic framework for INT1 and INT2-9 cells across feeding states, and to perform focused validation of selected candidates to establish the physiological relevance of the profiling results. We therefore view the current functional analyses as an initial validation and proof of principle, rather than a comprehensive mechanistic dissection of the molecular pathways for each candidate. We appreciate the reviewer's recognition that these findings provide an excellent starting point for future studies.

> *Appraisal of whether the authors achieved their aims, and whether the results support their conclusions:*
>
> *The main goal of the study was to survey the dynamic responses at the level of actively translated mRNAs of the INT1 vs INT2-9 cells in response to metabolic challenge.*
>
> *Overall, the authors use established methods to perform their genome-wide analysis, and the set of differentially regulated genes is enriched for expected molecular functions and forms coherent networks in anticipated pathways.*
>
> *The validation experiments (promoter::GFP fusion reporters, INT1-specific knockdowns of highly regulated genes) further corroborate the quality of the TRAP-seq datasets generated.*
>
> *I have a few points for the authors that would further strengthen this work:*
>
> *(1) The authors rightfully focus on the top differentially-regulated candidates, but it's unclear at present how far down their fold change list would lead to expression pattern validations. It would be useful to test a few more promoter::GFP fusion reporters at different enrichment/fold-change/statistical cutoffs.*

Testing additional promoter::mNeonGreen reporters across a wider range of fold-change and statistical thresholds could be somewhat useful for calibrating ranked TRAP-seq candidate genes. However, given the variation in strains bearing extrachromosomal arrays, we did not consider this a stringent enough test, given that the sensitivity and dynamic range of RNA-seq far outpaces genetic fluorescence-based reporters. For these reasons, we focused on the top differentially enriched candidates to provide not only an initial validation of the dataset, but also to determine whether these candidates regulate biological functions in INT1 cells and thus serve as potentially useful biological readouts in future efforts.

> *(2) Although the INT1-specific RNAi provides a convenient strategy for rapidly perturbing and testing genes of interest for phenotypes, independently validating the knockdowns with genetic mutants, or alternatively (if genes are essential), degron alleles.*

We agree that validating the INT1-specific RNAi phenotypes with independent genetic approaches, including null-allele or degron-based alleles for essential genes, would further strengthen the conclusions. In the current study, we used INT1-specific RNAi as a rapid and spatially restricted strategy to functionally test candidates identified by TRAP-seq and to determine whether these genes contribute to the specialized physiological functions of INT1 cells. We consider these experiments an initial validation of candidate function rather than a complete genetic dissection, which could be conducted in future efforts to study other aspects of INT1 function.

> *Impact:*
>
> *The TRAP-seq data and list of differentially-expressed candidate genes will form an interesting set of high-priority candidates to study for their role in the reception and transduction of nutritional cues in response to food status and pathogens. This data will thus benefit the C. elegans community of researchers studying the mechanisms governing these phenomena.*
>
> ***Recommendations for the authors:***
>
> ***Reviewer #1 (Recommendations for the authors):***
>
> *Major comments:*
>
> *(1) The authors need to describe the fasting method used in detail. Was fasting performed on unseeded NGM plates or in liquid (M9 buffer)? Were the animals washed with buffer prior to starvation? If yes, how many times? These details are critical for any researcher to follow up on their results.*

We have clarified the fasting/refeeding procedure in the revised Methods section. Briefly, worms were washed off OP50-seeded NGM plates with M9 buffer, washed three times in M9 buffer, and then transferred to unseeded NGM plates for fasting. For refeeding, worms were collected from the unseeded NGM plates with M9 buffer and transferred back to OP50-seeded NGM plates.

> *(2) The authors claim that "INT1 and INT2-9 cells maintain fundamentally different molecular identities independent of any and all acute or chronic conditions", which they primarily based on Principal Component Analysis (PCA). The circles shown in Figure 2A are arbitrary, and many such circles can be drawn in the 2D space to separate the samples in different ways. The authors should show this comparison in a translatome-wide similarity heatmap with hierarchical clustering (similar to Fig.2C, but with all the experimental conditions and their replicates on both x- and y-axes).*

The ellipses shown in Figure 2A were generated using the stat_ellipse() function in ggplot2, which calculates the mean and covariance of the PC1 and PC2 for each line and draws ellipses corresponding to the 95% confidence level. The separation between lines is primarily driven by PC2, which accounts for 14% of the variance in the translatomic dataset. Although this difference is less pronounced when considering the full translatome, samples from the same line nevertheless cluster together, supporting line-specific differences in translatomic profile.

> *(3) Figure 4 of the study shows 18 Venn diagrams for genes that are differentially expressed between INT1 and INT2-9 cell types in fed, fasted, and refed conditions. In the absence of any statistical comparisons, it is difficult to interpret whether the extents of overlap (higher or lower than expected) are significant. Ideally, P values for hypergeometric tests should be provided for the overlap regions.*

We appreciate the reviewer's suggestion. We explored the use of hypergeometric testing, implemented through the SuperExactTest package in R, to assess the statistical significance of

the overlaps shown in the Venn diagrams. However, this analysis yielded significant P values for essentially all overlap regions, including cases in which the degree of overlap was not especially informative and did not align with the interpretation presented in the text. This outcome likely reflects the dependence of the test on the size of the input gene sets and background universe, which can make statistical significance difficult to interpret meaningfully in this context.

> *(4) The claims made in lines 242-244 (Figure 5D) need to be supported by P values from hypergeometric tests.*

Similar to the previous point.

> *(5) The interpretation of Figures 6E and 6F described in lines 296-297 needs to be supported by statistical analyses. The authors claim that the undulating pattern of expression of the turquoise module genes is stronger in INT1 compared to INT2-9. However, based on Figures 2C and 6F, it appears that the expression change is not necessarily weaker in INT2-9, but instead is different, i.e., the expression of turquoise module genes goes up during fasting in INT1 and goes down after refeeding, while their expression goes up during fasting and stays up after refeeding in INT2-9 cells.*

We appreciate the reviewer's point and agree that the turquoise module shows dynamic regulation in both cell populations. The key difference is not the presence versus absence of an undulating pattern, but rather the magnitude of that change, which is greater in INT1. Because of the limited number of biological replicates in some conditions, particularly the fasting group, we interpreted these results cautiously and used a nonparametric approach to assess differences in average module expression between states. This analysis indicated that the turquoise module changes significantly in both lines, but with a larger effect size in INT1. We have included the corresponding statistical analysis and effect size in the revised manuscript.

> *(6) Since the INS-7 coelomocyte uptake assay was used extensively in this study, some representative microscopy images should be included to complement the quantification.*

We have added a new Figure 6G showing representative images corresponding to the quantification presented in Figure 6H.

> *(7) The authors claim that INT1-specific fmo-2 RNAi results in reduced basal INS-7 secretion, but they do not have the direct statistical comparison for this. Were experiments shown in Figures 6G and 6K done on the same day?*

In the original Figure 6K (now Figure 6L), the data are presented as the percentage of normalized INS-7::mCherry fluorescence intensity relative to fed animals treated with vector RNAi. A statistical comparison between fed animals treated with INT1-specific *fmo-2* RNAi and fed vector RNAi controls was performed and was significant. We have also clarified that the experiments shown in the original Figures 6G and 6I (now Figures 6H and 6J) were performed on the same day.

> *(8) It is not clear why blocking the mitochondrial breakdown of pyruvate (Figures 7E and 7F) does not mimic the fasted state in terms of increased INS-7 secretion from INT1 cells. Doesn't this contradict the proposed model in this study? Can the authors speculate why this is the case?*

We do not interpret inhibition of pyruvate dehydrogenase or pyruvate carboxylase as equivalent to the fasted state. Rather, our model is that fasting induces INS-7 secretion by lowering intracellular pyruvate in INT1 cells. Under this framework, blocking mitochondrial pyruvate breakdown would be expected to reduce pyruvate utilization and thus maintain intracellular pyruvate, preventing the drop in pyruvate that normally occurs during fasting.

This would explain why these manipulations suppress fasting-induced INS-7 secretion. To directly examine this possibility, we performed the experiment in Figure 7G, which tests whether maintaining pyruvate levels in INT1 cells during fasting is sufficient to suppress INS-7 secretion. The results are consistent with this interpretation and further support a model in which decreased intracellular pyruvate is a key determinant of fasting-induced INS-7 secretion.

> *Minor comments:*
>
> *(1) Figures 2E and 2G are very similar and represent the same result in two different ways (unbiased vs guided comparison). One of these should be moved to the supplementary figures.*

Although these figures show similar patterns, they were derived from two independent analytical approaches, WGCNA and differential expression analysis. We therefore interpret the concordance between these independent methods as strengthening the robustness of the association and increasing confidence in the biological relevance of the observed pattern.

> *(2) In Figures S1C, S1D, and S1E, a more significant P-value is shown with a smaller circle, and a less significant P-value is shown with a larger circle. This is confusing to the reader and should be inverted.*

We appreciate the reviewer's comment and have removed the original Figure S1C–E, replacing it with a more informative analysis. The genes used in the original panel were drawn from the top markers reported for intestinal clusters in Ghaddar et al. (PMID: 37352352). However, these markers were defined by comparison with all *C. elegans* cell types, rather than by comparisons among anterior, middle, and posterior intestinal populations, and are therefore not optimal for resolving differences between intestinal subregions. Our further examination of marker expression across the intestinal clusters in the Ghaddar et al. (PMID: 37352352). dataset confirmed this limitation. These results underscore the strength of our dataset for identifying genes that distinguish INT1 from INT2–9. We also note that the spatial identities of the intestinal clusters in Ghaddar et al. (PMID: 37352352) were not clearly established in the text or by spatial transcriptomic evidence, making it difficult to assign the annotated anterior, middle, and posterior clusters to specific intestinal cells. We have revised the manuscript accordingly and replaced the original figure panels.

> *(3) Line 131 mentions the comprehensive characterization of the translatomic differences between INT1 and INT2-9 cells under each acute and chronic condition. However, the paragraph only discusses the differences in the fed condition. This is confusing, and the authors should mention the comparison between these cell types under acute and chronic conditions in subsequent sections where it is described.*

In this paragraph, we indeed discuss the 'fed' condition, but in subsequent sections we follow with details analyses of acute versus chronic, as well as regional differences across the intestine. We have clarified this in the opening sentence of the referenced paragraph.

> *(4) The Venn diagrams in Figure 4 look very similar, and it is hard to differentiate between how 4A is different from 4I, how 4B is different from 4J, etc. The authors should include the labels for 'acute' or 'chronic' above each Venn diagram to guide the reader through these panels.*

We have added labels indicating the acute and chronic conditions to the left side of each Venn diagram in the revised Figure 4.

> *(5) It is not clear in the figure legends how Figure 5E is different from Figure S6A, and how Figure 5F is different from Figure S7A. This should be better described in the figure legends.*

We have added a sentence to better describe this in the figure legend.

> *(6) Figure 6C: Survival parameters such as median lifespan, number of animals for each condition, etc., should be reported for the different conditions.*

We have revised Figure 6C to indicate the number of animals analyzed in each condition, and the median survival for each group is now reported in the corresponding figure legend.

> *(7) The colors used for control RNAi and clec-160 RNAi are very similar in Fig.6C. Easily distinguishable colors should be used.*

We have changed the colors as suggested.

> *(8) The INT1-specific RNAi strain should be first described in line 285.*

We have added the description for the INT1-specific RNAi strain in line 285.

> *(9) Line 304: 'REF' should be replaced with the reference.*

We have replaced the “REF” with the reference (PMID: 39127676)

> *(10) The P value for statistical comparison between the fed and 30 min refed states should be shown in Figures 6G, 6I, and 6K.*

We have now included the *p* value for the comparison as suggested. Figures 6G, 6I, and 6K are now labeled as 6H, 6J, and 6L, respectively.

> *(11) In Figure 7, the authors should consider replacing the 'refed' label with 'recovery' because the pyruvate treatment was done in the absence of 'feeding' (= bacteria consumption).*

We appreciate the reviewer’s point. However, we chose to retain the label “refed” in Figure 7 to maintain consistency across the set of conditions examined, including 2% glucose and OP50 supernatant, which likewise do not involve bacterial consumption despite not showing effect on the refeeding response of INS-7 secretion.

> *(12) The full form of DISN should be mentioned in the figure legend of Figure 7.*

We have included the full form of D1SN in the figure legend of Figure 7A.

> *(13) Line 367: 'normalization' should be replaced with 'return to basal levels'. 'Normalization of INS-7 secretion' might also mean normalization of INS-7::mCherry signal to CLM::GFP signal.*

We have revised the wording per the reviewer's suggestion.

> *(14) The methods section has a quantitative RT-PCR section, but it is not clear if RT-PCR data are reported in any of the figures. Also, no qPCR primers are listed in Table S3.*

We have removed the quantitative RT-PCR part from the methods section.

> ***Reviewer #2 (Recommendations for the authors):***
>
> *(1) The authors describe that the RPL-22-3xHA constructs are not integrated, at the very end, in the section "Limitations of the data". An earlier mention of this caveat would have been useful. In addition, it would help if the authors could provide their defense (which I think is very valid) of using non-integrated strains in the results section, as they describe the experimental setup. Also, some details were missing, which left me wanting to know:*

> *Were there expression differences? How were they accounted for? Was expression normalized between these two constructs, and if so, how?*

The RPL-22-3xHA construct was integrated into each line to ensure more consistent transgene expression across experiments. Because the INT2-9 construct is expressed in a larger number of cells than the INT1 construct, the INT2–9 samples yielded greater amounts of pulled-down nascent RNA, as reflected in the supplemental table and in the higher aligned RNA counts observed for the INT2-9 samples. To account for these differences, differential expression analysis was performed using DESeq2, which corrects for library size by estimating sample-specific size factors with the median-of-ratios method. Raw counts are then normalized using these size factors, thereby accounting for differences in sequencing depth and minimizing confounding effects due to variation in library size. Such differences are common in RNA-seq experiments, particularly when comparing samples derived from distinct input populations.

> *(2) The 'acute' and 'chronic' exposures are thought through and carefully defined. The question I do have is whether the 3-hour fasting can be considered chronic fasting, given how surprisingly fast the animals lose their fat content. Could these kinetics indicate that the 30-minute fasting is reflective of mechanisms during which senses change in food availability, whereas the 30 minutes represents acute fasting (with chronic fasting - meaning fasting, during which the animal activated alternative pathways - occurring later)? While this may appear to be pure semantics, it could influence how the authors interpret their results. One method to more objectively separate an 'acute' from a 'chronic' stage may be to conduct a time course of fat loss-does fat loss plateau after 3 hours? The timing when the rate of decrease levels off could be more indicative of the beginning of a chronic phase.*

We appreciate this important point and agree that it should be more clearly discussed. We interpret acute fasting as a pre-fat-loss state, since it is 30 minutes off food and no difference in fat levels are detectable at this stage (Fig 1B). The translatomic changes observed under acute fasting therefore likely reflect food-sensing mechanisms and early preparatory responses that promote subsequent fat mobilization. In contrast, chronic fasting (180 minutes off food – see Fig 1D) appears to represent a post-fat-loss state, in which fat stores have already been depleted, and the corresponding translatomic changes likely reflect the effects of sustained metabolic stress.

> *(3) The age of the animals used has to be more explicitly stated. Were these animals egg-laying? Or L4/young adults? This is likely to impact the changes that the animals undergo.*

Day 1 young adults were subjected to the fasting. Great care was taken to ensure consistency across biological replicates.

> *(4) What is the rationale, in the authors' view, that stress response genes are apparently more enriched than metabolic or mitochondrial enzymes, and membrane receptor changes? Are the latter mostly regulated by PTMs/localization changes, etc?*

Based on our current data, we cannot exclude the possibility that metabolic or mitochondrial enzymes, as well as membrane receptors, are regulated in INT1 and INT2–9 cells through mechanisms not captured at the translatome level, including post-translational modification or changes in subcellular localization under different fasting and refeeding conditions.

> *(5) The refeeding experiment with latex beads and killed OP50 is very clever. Details on when INS-7 was evaluated in the caoelomocytes would help the reader better understand and interpret these results.*

INS-7mCherry signal was evaluated in the coelomocytes immediately after refeeding; we included this information in the methods section and referenced our previous paper.

> *(6) In the Discussion, I was looking for a more detailed context for how to think about the differences and similarities in the RNA-seq data between the two segments, and perhaps a discussion of whether there were any indications that the two segments communicated with each other.*

The data show that the most pronounced difference between INT1 and the rest of the intestine at the RNAseq level, is the expression of stress response genes in INT1. Although there are some nuanced differences, the prevalence of stress response genes persists across feeding and fasting conditions. This difference, combined with the evidence that INT1 cells secrete the enteroendocrine peptide INS-7 (Fig 6 and PMID: 39127676) is strongly reminiscent of the mammalian enteroendocrine cells, which also secrete peptides and show strong expression of stress response genes (PMID: 37626258 and 27148273). We suggest that this category term reflects not only a canonical stress response, but also a broader response to shifts in the luminal environment, which INT1 cells are anatomically poised to detect well before the absorption of nutrients has begun further down the intestine (INT2-9). Thus, we believe INT1 cells are a newly defined enteroendocrine cell type within the *C. elegans* intestine.

Regarding communication between INT1 and INT2-9 – this is an intriguing possibility that we have considered, given that peptide genes and receptors are found in the RNAseq datasets. The extent to which the expression of these genes leads to functional effects is the subject of future investigation.

> ***Reviewer #3 (Recommendations for the authors):***
>
> *(1) Figure 1A - It would be better to also show single fluorescent protein channels to assess the specificity of the expression patterns. A schematic or labels of where the INT1 vs. INT2-9 boundaries are located would be helpful to non-experts.*
>
> *(2) Figure 4 - At present, the Venn Diagrams are a very complicated way to visualize all of the comparisons/conditions. I would recommend that the authors consider using UpSet plots to better summarize the relevant comparisons they would like to make. The same consideration applies to Figure 5D.*
>
> *(3) Line 301 - Description of the INT1-specific RNAi strategy. I think it would be better to bring this information earlier, close to line 285, where the authors first mention performing INT1-specific RNAi experiments.*

We have added the description for the INT1-specific RNAi strain in line 285.

> *(4) Line 304 - I think the authors meant to cite a reference where the REF placeholder text is found*

We have replaced the “REF” with the reference.

https://doi.org/10.7554/eLife.109237.2.sa0